LBL--14719

DE83 001037

MODE SPECIFICITY IN UNIMOLECULAR REACTION DYNAMICS

By

Boyd Alan Waite
(Ph.D. Thesis)

Lawrence Berkeley Laboratory
University of California
Berkeley, California 94720

July 1982

This work was supported by the Director, Office of Energy Research, Office of Basic Energy Sciences, Chemical Sciences Division of the U.S. Department of Energy under contract number DE-AC03-76SF00098. Also, all calculations reported were performed on a Harris H800 minicomputer, funded by National Science Foundation Grant CHE-79-20181.

To Jeanene, Scott, Erin, John, and future children

TABLE OF CONTENTS

Page

Dedication ii

Acknowledgements vii

I. Model Studies in Unimolecular Reaction Dynamics . . 1

A. A Phenomenological Example 4

B. A Model for Unimolecular Decomposition 6

C. Quantum Mechanical Calculations 12

1. The Complex Scaling Method 12

2. Calculations and Observations 17

D. A Classical Trajectory Approach 19

1. Probability Branching Model 20

2. Initial Conditions 24

3. Results and Observations 29

II. The Henon-Heiles Potential Energy Surface 32

A. Quantum Mechanical Calculations 34

B. Observations 38

1. Symmetry-induced Mode Specificity 38

2. The Classical Limit 40

C. A One-barrier Henon-Heiles Potential 43

D. Discussion 45

Page

III. A Semi-classical Multi-channel Branching Model . . . 47

A. General Development of the S-Matrix 49

B. Application to Unimolecular Decomposition . . . 53

C. Dynamical Approximations 58

D. Calculations for Model Unimolecular Systems . . 65

E. Other Applications of the Branching Model . . . 67

1. Energy Levels in a Multi-dimensional Double Well Potential 67

2. Reaction Probabilities in Complex Formation 72

IV. Mode Specificity in Formaldehyde Decomposition . . . 76

A. The Hamiltonian 80

B. Dynamical Results 83

C. Effects of Other Modes 87

D. Discussion 88

References 90

Tables 97

Figure Captions 101

Figures 106

MODE SPECIFICITY IN UNIMOLECULAR REACTION DYNAMICS

BOYD ALAN WAITE

ABSTRACT

Theoretical studies on mode specificity in unimolecular reaction dynamics are presented, based on essentially exact quantum mechanical methods (viz., the complex scaling method), a semi-classical multichannel branching model, and classical trajectory methods. The principal aim is to discover the relevant factors governing whether a unimolecular system exhibits mode specificity in its individual state rate constants, i.e., whether quasi-degenerate metastable states decay with significantly different rates. Model studies of two nonlinearly coupled oscillators (one of which can dissociate) demonstrate the effects of various features of potential energy surfaces on the character of the rates (e.g., degeneracy of modes, reaction path curvature, frequency modulation, etc.). These results and those obtained for the Henon-Heiles potential energy surface indicate an apparent absence of correlation between the quasi-periodic/ergodic motion of classical mechanics and the mode specific/statistical behavior of the unimolecular rate constants.

A different type of mode specificity, i.e., a symmetry-induced mode specificity, is demonstrated for systems possessing some degree of symmetry along the reaction path. States belonging to different irreducible representations may display significantly different rates,

even though there may be statistical-like behavior within a given representation.

In order to deal with the question of mode specificity in more realistic polyatomic systems, a semi-classical multi-channel branching model is developed, with dynamical approximations based on the reaction path Hamiltonian and the semi-classical perturbation-infinite order sudden approximation. The model is applied with success to a state-specific unimolecular decomposition system, as well as other polyatomic dynamical processes.

Finally, a study of the formaldehyde unimolecular decomposition is presented, with attention focused on the unique role of the out-of-plane bend in determining the mode specific character of the decay rates. Results indicate that both symmetry-induced mode specificity and dynamical mode specificity (i.e., within a given irreducible representation) are present in this system.

ACKNOWLEDGEMENTS

The completion of the research contained in this dissertation could not have been accomplished without the extraordinary scientific insights and direction of Professor William H. Miller. His initial suggestion to pursue the question of mode specificity in unimolecular reaction dynamics has proven to be most fruitful, enabling my entire graduate career to pass by without serious set-backs or discouragements. In addition, I wish to thank the many members of the Miller research group with whom it has been my privelege to associate these past several years. Their varied backgrounds and interests have both amused and aided me immensely. A special thanks should be included to Bishop J. Grant Chamberlain and other associates for the tremendous moral support they have given me, and for giving me an opportunity to spend time thinking about other things, keeping me in contact with the realities of life. Finally, and most importantly, I thank my wife Jeanene for making my life and the lives of our three children so meaningful and happy. She has borne the greatest burdens of all, and has succeeded admirably.

I acknowledge financial support from the Director, Office of Energy Research, Office of Basic Energy Sciences, Chemical Sciences Division of the U. S. Department of Energy, under contract number DE-AC03-76SF00098. Also, all calculations reported were performed on a Harris H800 minicomputer, funded by National Science Foundation Grant CHE-79-20181.

I. Model Studies in Unimolecular Reaction Dynamics

The modern theories of unimolecular reaction rates have their foundations in the famous Lindemann Mechanism[1], first proposed in 1922, which has the following kinetic scheme:

$$A + M \xrightarrow{k_a} A^* + M \quad \text{(activation)} \qquad (1.1a)$$

$$A^* + M \xrightarrow{k_d} A + M \quad \text{(deactivation)} \qquad (1.1b)$$

$$A^* \xrightarrow{k(E)} \text{products} \quad \text{(reaction)} \qquad (1.1c)$$

The molecular species to undergo unimolecular reaction is represented by A, its internally excited (or activated) form by A^*, and M represents some colliding partner. The rate coefficient $k(E)$ in Eq. (1.1c) depends on the total internal energy E and (in the general case) the initial distribution of that energy among the internal states.

Theoretical interest[2] has focused on the third step (Eq. 1.1c), where an activated molecule undergoes energy redistribution until sufficient energy is localized in the relevant reactive mode, whereupon reaction occurs. The nature of the theoretical treatments or models describing the process in Eq. (1.1c) has taken various forms.[2] The most successful of these[2c] have been founded upon statistical theories, similar in spirit to those employed in conven-

tional transition state theory[3] for bimolecular collisions. In fact, this statistical approach (i.e., the RRKM theory[2]) for treating unimolecular reactions can be shown to be the microcanonical ensemble analogue of transition state theory.[4]

For the process (Eq. (1.1c)), the RRKM expression for the rate coefficient k(E) has the following form:[5]

$$k(E) = \frac{N(E)}{2\pi\hbar\, N'_o(E)} \qquad (1.2)$$

where N(E) and $N_o(E)$ are the integral densities of states for the transition state (or activated complex) and for the reactant molecule, respectively.

When this expression is incorporated into the overall mechanism of Eq. (1.1), experimental results are reproduced with very great success for many polyatomic systems.[6a] This success has led many workers in the field of unimolecular reactions to the conclusion that, at least for most polyatomic systems, the underlying assumptions of the RRKM theory are valid,[6b] these assumptions being that (1) internal energy of the activated molecule is redistributed among all the internal degrees of freedom on a time scale fast compared to unimolecular reaction, and (2) all internal states of the molecule are accessible and ultimately lead to products.[7]

It has only been in recent years that experimental technology has allowed for direct testing of the validity of these assumptions.[8] For instance, the possibility of exciting the molecular species in

the activation step (Eq. (1.1a)) to some specific state (e.g., via a local mode overtone excitation with a laser) might lead to some type of mode specific behavior. The assumptions of the RRKM theory preclude the possibility of such behavior in that the excited system must immediately lose its memory (due to rapid intramolecular relaxation) as to which particular mode was initially excited. In other words, within the RRKM picture, the rate constant $k(E)$ for the process in Eq. (1.1c) can only depend upon the total internal energy, and not upon the initial distribution of that energy. Throughout the remainder of this work, such behavior in the rates will be referred to as statistical behavior.

If a molecule is excited in a specific way, as is possible with a laser, and if we consider an isolated, collisionless molecular system, then the basic question to be addressed is whether or not unimolecular chemistry (i.e., product formation) will occur before intramolecular relaxation processes destroy the specificity of the excitation. Stated another way, one asks if the rate of the reaction (Eq. (1.1c)), or other characteristics of the reaction such as product distributions, depends not just on the amount of excitation energy but on the specific way this energy is put into the molecule, i.e., on which modes are excited.

As an extreme example of unimolecular behavior, consider the formation of Van der Waals complexes in a molecular beam.[9] For a given amount of vibrational energy in $I_2 \cdots He$, for example, it is clear that the rate of decomposition depends on whether the energy

is initially in the vibration of the I_2 molecule or in the weak Van der Waals bond. Such a system would be said to exhibit mode specific character in its decay rates. For more normal molecules, however, such obvious characterization of the rate behavior is not possible, and it has been commonly assumed that mode specific effects are unimportant for such systems. Several recent experimental studies,[10] however, claim to have observed such mode specific effects in "typical" unimolecular systems (e.g., allyl isocyanide isomerization[10a]).

A. A Phenomenological Example

Recent theoretical work related to mode specific chemistry has taken two directions. One approach[11] has been concerned with the question of ergodicity as it relates to intramolecular dynamics, there being a seemingly natural connection between the ideas of chaotic behavior and the statistical assumptions of the RRKM theory. Many attempts have been made at establishing a connection between classical and quantum mechanical ergodicity in hopes of being able to describe the relevant features of the intramolecular dynamics. A second approach, the one to be followed in this presentation, considers more directly the dynamics of the unimolecular reaction. That this approach should be more fruitful in dealing with the question of mode specificity in unimolecular reaction dynamics is seen in the following phenomenological example.

Consider an elementary two-state model of unimolecular reaction, whose kinetic scheme is as follows:

$$1 \underset{k_{in}}{\overset{k_{in}}{\rightleftharpoons}} 2 \qquad (1.3a)$$

$$1 \xrightarrow{k_1} \text{products} \qquad (1.3b)$$

$$2 \xrightarrow{k_2} \text{products} \qquad (1.3c)$$

The rate of intramolecular transfer between "states" 1 and 2 is k_{in}, and "states" 1 and 2 react at rates k_1 and k_2, respectively.

Solving for the eigenvalues of the resulting set of master equations yields the following intrinsic reaction rates:

$$\text{rate} = (k_1 + k_2)/2 \pm \frac{(\frac{k_1 - k_2}{2})^2}{k_{in} + \sqrt{k_{in}^2 + (\frac{k_1 - k_2}{2})^2}} \qquad (1.4)$$

This system is ergodic by construction, i.e., it spends the same amount of time in each of the states 1 and 2 due to the equal rates of hopping back and forth between the states. The statistical rate, i.e., $(k_1 + k_2)/2$, however, is obtained only in the limit

$$k_{in} >> \left| (\frac{k_1 - k_2}{2}) \right|$$

which, of course, corresponds to the standard RRKM assumptions. In the opposite limit the system is mode specific with rates given by

k_1 or k_2, even though the intramolecular dynamics is ergodic. The relevant result of this simple phenomenological example is that the approach of considering only the intramolecular dynamics may lead to erroneous conclusions regarding the unimolecular dynamics. In other words, whether the intramolecular dynamics is formally ergodic or not in the infinite time limit does not seem as relevant to mode specificity as does the rate of intramolecular energy transfer compared to the rate of the chemistry of interest.

B. A Model for Unimolecular Decomposition

The simplest model of unimolecular decomposition is a system of two coupled oscillators, one of which can dissociate. The object in studying such a simple model would be to calculate the unimolecular reaction rates associated with it, and then, by varying the relevant parameters of the potential energy surface, see which are most important in distinguishing between mode specific and statistical behavior. Past studies[12] of such coupled oscillator systems, however, have shown that for energies above the classical threshold for reaction the molecule decomposes too fast for any amount of coupling between the oscillators to yield the purely statistical limit. In order to overcome this difficulty inherent in two oscillator models, it is necessary to choose the dissociative oscillator to have a potential barrier to dissociation so that the reaction must proceed by tunneling. By varying the size of $\hbar$ (which is arbitrary for a model system), one

can thus slow down or speed up the rate of dissociation without significantly affecting the intramolecular vibrational dynamics. Thus one might be able to find a system of two oscillators which exhibits the necessary balance between intramolecular relaxation rates and unimolecular reaction rates necessary for statistical behavior in the overall decay rates.

The Hamiltonian for the two-oscillator system to be considered is

$$H = \frac{p_x^2}{2m} + \frac{p_y^2}{2m} + V_1(x) + \frac{1}{2} m\omega_y^2 y^2 + V_c(x,y) \qquad (1.5)$$

where $V_1(x)$ is a potential function as shown in Fig. 1, and V_c is the interaction which couples the two oscillators. Such a system has only metastable or quasibound vibrational states, which are characterized by complex energies, $E_r - i\Gamma/2$, as is well known from resonance scattering theory.[13] The real part of the complex energy E_r is the energy of the metastable state, and the imaginary part is related to its lifetime τ and the unimolecular decay rate k by

$$k = 1/\tau = \Gamma/\hbar \qquad (1.6)$$

The determination of the state specific unimolecular decay rates for such a system would consist of calculating the complex energies for all the quasibound states. Inspection of the resulting decay rates considered as a function of energy would then indicate whether the

system was mode specific or statistical in its rate behavior.

To demonstrate this scheme for evaluation of unimolecular systems, it is illustrative to consider first the uncoupled case, i.e., $V_c = 0$ in Eq. (1.5) . The complex energies are then characterized by a quantum number for each oscillator and are additive:

$$E_{n_x,n_y} = (\varepsilon_{n_x} - i\Gamma_{n_x}/2) + \varepsilon_{n_y} \qquad (1.7)$$

Note that in this uncoupled limit, only the energy of the x-mode is complex. The energy E and the rate constant k for the quasibound state with quantum numbers n_x and n_y are then

$$E_{n_x,n_y} = \varepsilon_{n_x} + \varepsilon_{n_y} \qquad (1.8a)$$

$$k_{n_x,n_y} = \Gamma / \hbar \qquad (1.8b)$$

This represents the extreme of mode specificity; the energy, once deposited in a given mode, remains isolated in that mode. The rate of decay depends only on the quantum number (and thus the energy) of the x-mode. By plotting the individual state rate constants k_{n_x,n_y} versus total energy E_{n_x,n_y} , as in Fig. 2 , this mode specific or non-statistical character is dramatically evident. For a statistical or RRKM-like system, k should be a smooth monotonically increasing function of the total energy E , and the present uncoupled system depicted in Fig. 2 is clearly the opposite extreme.

An interesting observation connecting this uncoupled (or weakly coupled) picture to standard RRKM rate expressions can be made as follows. Consider the limit of many closely spaced energy levels in an uncoupled system (as in Fig. 2) and compute the <u>average</u> rate constant at energy E,

$$k(E) \equiv \frac{\sum_{n_x,n_y} k_{n_x,n_y}\, \delta(E - E_{n_x,n_y})}{\sum_{n_x,n_y} \delta(E - E_{n_x,n_y})} \tag{1.9}$$

where in actuality the δ - functions should be broadened so that at least several quasibound states have energies within their width about energy E. Such an average may be significant, even for very weakly coupled systems, if the method of activation of the molecule is not state specific.

By invoking the separability of the energy (Eq. (1.8a)) as well as the semi-classical approximation [14] for Γ_{n_x}, i.e.,

$$\Gamma_{n_x} \simeq P(\varepsilon_{n_x})\, (\partial \varepsilon_{n_x} / \partial n_x)/ 2\pi \tag{1.10}$$

where $P(\varepsilon_{n_x})$ is the one-dimensional tunneling probability for the x-mode, and by going to the continuum limit

$$\sum_{n_x} \rightarrow \int dn_x \tag{1.11}$$

it is easy to show that the average rate of Eq. (1.9) is just

$$k(E) = \frac{1}{2 \pi \hbar \rho(E)} \sum_{n_y} P(E-\epsilon_{n_y}) \qquad (1.12)$$

which is recognized as the RRKM rate expression including tunneling.[15] (Note that $\rho(E)$, in the denominator of Eq. (1.12), is just the density of quasibound states.) Thus, the average rate constant at total energy E is just the RRKM statistical rate even in the case of no coupling between the modes. Even if there is coupling between the modes, it is still possible to define an average rate $k(E)$ for a given total energy by averaging the individual rate constants over some energy interval.

The scheme outlined above for describing unimolecular reaction rates, therefore, is to construct decay rate profiles such as that of Fig. 2 for systems in which V_c is not zero. The fundamental question with regard to mode specificity is, when coupling between the modes is introduced, do all the points in Fig. 2 move and fall along a single smooth monotonically increasing curve (i.e., the curve $k(E)$ of Eq. (1.12)). In other words, are there systems for which the unimolecular decay rates of each individual quasibound state depend only on their total energy. To investigate the extent to which this does or does not occur is the purpose of the model calculations described in section I.C.

To be more specific, the particular functional forms used for the potentials in the Hamiltonian of Eq. (1.5) are

$$V_1(x) = \frac{1}{2} m \omega_x^2 x^2 e^{-x^2} \tag{1.13a}$$

$$V_c(x,y) = x^2 e^{-x^2} \left(V_2 y - \eta \frac{m \omega_y^2}{2} y^2 \right) \tag{1.13b}$$

The potential energy is harmonic near the bottom of the well with frequencies ω_x and ω_y, and through cubic anharmonicities it is identical to the well-studied Barbanis potential.[16] Thus, results of calculations for this system should give some clues as to whether the classical ergodic features of the system (which the Barbanis system is known to possess) are relevant to the mode specificity of the unimolecular rates.

The coupling interaction in Eq. (1.13b) has two terms. The η coupling serves to dilute or modulate the transverse frequency as one moves along the reaction path from reactants to products. Its effect (which is typical in many chemical systems) is to effectively widen the valley leading to products in the transition state region, i.e., the region of loosely bound complexes. The V_2 - type of coupling of Eq. (1.13b) introduces curvature in the reaction path, i.e., the path of steepest descent down from the saddle points. These are the two types of coupling present in real systems, and one would like to ascertain which is most closely associated with mode specific or statistical behavior. Finally, by varying the degree of degeneracy

between the two modes, i.e., by varying the frequencies ω_x and ω_y, it should be possible to determine the effect on the mode specific character of the decay rates of resonant versus non-resonant intramolecular energy transfer.

C. Quantum Mechanical Calculations

1. The Complex Scaling Method[17]

The quasibound states associated with unimolecular decomposition are characterized by complex energies

$$E_r - i\,\Gamma / 2 \tag{1.14}$$

where E_r is associated with the energy of the state and Γ is, as discussed in section I.B, related to the decay rate or inverse lifetime of the state. That this is the case is seen most directly by noting that the time dependent Schrodinger equation for complex energies

$$i\,\hbar\,\frac{\partial\psi(x,t)}{\partial t} = H\,\psi(x,t) = (E_r - i\Gamma/2)\,\psi(x,t) \tag{1.15}$$

leads to probability distributions

$$|\,\psi(x,t)\,|^2 = |\,\psi(x,0)\,|^2\, e^{-\Gamma t/\hbar} \tag{1.16}$$

which decay exponentially with rate coefficient $\Gamma / \hbar$.

The complex energies of metastable states are defined rigorously as the poles of the analytically continued Green's function,[13] or equivalently of the S - matrix (i.e., by considering the metastable states to be resonance states in a scattering situation). These resonance states give rise to resonance peaks in a scattering experiment measuring total cross sections, the width of the peak being associated with the imaginary part of the complex energy. Finally, and perhaps most directly, the complex energies are defined as the eigenvalues of the time independent Schrodinger equation with boundary conditions imposed on the wave function of out-going waves only.[18] Since such boundary condition constraints give rise to non-Hilbert space type of wave functions, the Hamiltonian operator is no longer Hermitian, therefore giving rise to complex eigenvalues.

Over the years, there have been many approaches to calculating these complex energy eigenvalues, both by approximate methods[19] and by essentially exact quantum mechanical methods.[18] Recently, several new methods have appeared which apply variational methods similar to those used for ordinary bound state calculations. For example, the Siegert eigenvalue approach,[18] which applies the out-going wave boundary contition directly, has been used with some success in treating electron-atom resonances.[20] One of the difficulties associated with this approach, however, is that each metastable state for the system must be obtained separately. For a unimolecular decomposition model such as that given in section I.B , where many quasibound

states exist, such a procedure would be prohibitive computationally.

The complex scaling method,[17] which is closely related to the Siegert eigenvalue approach, is more convenient for the purposes at hand since it permits the calculation of many eigenvalues simultaneously. Though the mathematical justifications[17] for the method are beyond the scope of this work, the physical idea underlying the method is clear. First, a transformation of the Hamiltonian is made by scaling the coordinates $\underset{\sim}{x}$ by a complex factor:

$$\underset{\sim}{x} \rightarrow \underset{\sim}{x} \exp(i\,\theta) \tag{1.17}$$

so that

$$H(\underset{\sim}{x}) \rightarrow H(\underset{\sim}{x} \exp(i\theta)) \equiv H_\theta \tag{1.18}$$

Note that the kinetic energy operator scales as $d^2/dx^2 \rightarrow$ $\exp(-2i\theta)\, d^2/dx^2$.

Such a transformation has the following effects on the spectrum of energy eigenvalues: (1) bound state eigenvalues (if any) are unchanged, (2) continuum eigenvalues are rotated down in the complex energy plane by an angle 2θ , and (3) metastable complex eigenvalues (if any) are unchanged except that for sufficiently large angles of rotation, they are now resident upon the first energy sheet, having been effectively "uncovered" due to effect (2) above (the continuum

energies form the branch cut separating the two Riemann sheets[21]. One then proceeds to solve the Schrodinger equation

$$H_\theta \chi = (E_r - i \Gamma/ 2) \chi \qquad (1.19)$$

by conventional bound state techniques, i.e., by expanding the wave function χ in a suitable basis set and diagonalizing the resulting complex symmetric matrix. In essence, the complex scaling method transfers the non-Hermiticity of the system from the boundary conditions on the wave function to the Hamiltonian operator itself, thereby allowing one to expand the new wave function in a more convenient bound state type of basis set.

Recent work[22] on the complex scaling method has shown that in a system with both dissociative and bound degrees of freedom it is only necessary to scale the coordinates associated with the dissociative degree of freedom. That this should be the case is seen by considering the fact that the complex scaling factor introduces oscillatory character into the basis functions, a correct feature for dissociative wave functions, but not so appropriate for the bound degree of freedom wave functions.

By employing the transformation (Eq. (1.18)), the Hamiltonian for our model system becomes

$$H_\theta = - \frac{\hbar^2}{2m} e^{-2i\theta} \frac{d^2}{dx^2} - \frac{\hbar^2}{2m} \frac{d^2}{dy^2} + V(xe^{i\theta} , y) \qquad (1.20)$$

where V is the potential energy function of Eqs. (1.13) . For the calculations to be presented in section I.C.2 , the wave function χ is expanded as follows:

$$\chi = \sum_{n_x,n_y} C_{n_x,n_y} \phi_{n_x}(x) \xi_{n_y}(y) \tag{1.21}$$

where $\phi_{n_x}(x)$ and $\xi_{n_y}(y)$ are harmonic oscillator basis functions. (Other types of basis sets were tried, including a coherent states basis set[23], with no significant difference in convergence properties.)

All matrix elements were computed using double precision word size so as to insure stability sufficient to obtain resonances with widths as small as 10^{-20} . In addition, all the computations reported in section I.C.2 used 40 basis functions for the dissociative degree of freedom and four basis functions for the bound degree of freedom. Truncation of the basis set expansions leads to slight dependence of the complex eigenvalues on the angle of rotation θ . Typically, regions of stability of angle trajectories have been sought be either graphical methods or complex Hellmann-Feynman theorems,[24] whereas in these computations the imaginary parts of the eigenvalues were found to be stable to at least three significant figures (some to as many as eight) over at least five degrees of rotation. This broad band of stability enabled all the complex eigenvalues (i.e., all the quasibound states) to be obtained simultaneously.

2. Calculations and Observations

The object of the calculation of metastable state decay rates for the model system (Eq. (1.5)) is to ascertain the effects of various types of intramolecular coupling on the mode specificity of the decay rates. Table I gives the values of the various coupling parameters investigated, results of which are presented in the following paragraphs.

Zero Coupling Limit. Fig. 2 is the system with zero coupling as discussed in section I.B . This represents the extreme limit of mode specificity.

Frequency Dilution and Curvature. Figs. 3 and 4 illustrate the effects of the two types of coupling (frequency dilution for Fig. 3, curvature for Fig. 4) taken separately. It is clear from both systems that neither type of coupling alone results in significant statistical behavior. There is some tendency of the individual rates to coalesce along a single monotonically increasing curve, but these two systems are still highly mode specific. Fig. 5 presents a system combining the two effects, with the same strengths as for the systems of Figs. 3 and 4 separately. It is obvious from Fig. 5 that their effects on the rates are non-additive, i.e., their combined effect is to produce a system which is substantially more statistical than either of the two taken individually.

Intramode Degeneracy. Figs. 6, 7, and 8 illustrate the effects of intramode degeneracy upon the energy randomization process. Increased degeneracy between modes is expected to enhance the resonant

energy transfer between modes, thus resulting in greater randomization and "equal weighting" of all contributing states (see section I.B). Fig. 7 represents the highest degree of degeneracy of the three systems (taking into account the anharmonicity of the x-mode), and along with the couplings present leads to a strikingly statistical rate constant profile.

Effects of Ergodicity. An interesting observation of these quantum mechanical systems discussed thus far is that there seems to be no energy requirement for statistical behavior in the unimolecular rates. In other words, for these quantum systems, statistical behavior is seen to occur at low energies to essentially the same extent that it occurs at higher energies. Classically, these types of coupled oscillator systems are known to often exhibit a definite transition[16] from quasi-periodic trajectories to chaotic (or ergodic) trajectories as energy increases. This apparent disparity in quasi-periodic/ergodic and mode specific/statistical behavior between classical and quantum mechanical treatments is even more clearly illustrated by the system of Fig. 9, which was chosen to be one that exhibits a well-defined classical stochastic transition. Fig. 9 shows, as for the other systems, the specific rates as a function of energy. The vertical dashed line at the lower energy indicates the onset of the classical stochastic behavior (as determined from Poincare Surfaces of Section[25]), and the line at the higher energy indicates the top of the barrier. The specific rate constants show no more (or less) mode specific character below the stochastic transition than they do

above it. In other words, there appears to be no specific correlation between the classical behavior and the character of the quantum decay rates.

That these two approaches to characterizing the unimolecular dynamics are actually monitoring different phenomena is seen from the following discussion. For the classical case the lifetime is infinite no matter what energy the particle (so long as it is below the classical threshold), i.e., the system has an infinite amount of time to decide whether or not it is going to be ergodic at all energies. In considering unimolecular decay of the quantum system, on the other hand, even though the rate of intramolecular energy transfer increases with increasing energy, so does the rate of unimolecular decomposition, so that the system has less time to randomize its internal energy before dissociation. It is thus not unreasonable for the degree of statistical behavior in the unimolecular rates to be similar for all energies, and for the systems depicted in Figs. 2-9, this is approximately the case.

D. A Classical Trajectory Approach

The quantum calculations presented in section I.C are, of course, the exact results for the given model systems. Such calculations would not be practical, however, for real molecular systems, which have more than two degrees of freedom. Therefore, it is of considerable interest to develop simpler approaches that, although less

accurate, can be applied to more general types of chemical systems.

Classical trajectory methods[26] have been developed extensively such that nowadays such simulations can be carried out routinely for small polyatomic molecules (provided a potential energy surface is available). With reference to unimolecular dynamics, classical trajectory simulations can only be useful at total energies above the classical barrier height for dissociation, and many such calculations have appeared.[27] The object of this development is to combine the classical trajectory method with an approximate semi-classical tunneling model in order to extend the conventional trajectory methods to the energy region below the classical barrier height, as is the case for the model studies presented in section I.C. Not only does this model serve to compare with the quantum results, but it also will be directly applicable to such unimolecular processes as formaldehyde decomposition, which is postulated to proceed via tunneling based upon some experimental results[28] and other theoretical considerations.[29]

1. Probability Branching Model

The basic physical idea of the approach is very simple: A classical trajectory is begun inside the potential well, and since the energy is below the barrier height, it will oscillate in the well forever. Each time the trajectory hits the barrier (i.e., experiences a classical turning point along the barrier direction), however, it is allowed to tunnel through it with a probability computed from the local properties of the trajectory at that time. The probability that

by time t the particle has not tunneled out, i.e., the survival probability, is

$$P_s(t) = (1-P_1)(1-P_2) \cdots (1-P_{K(t)}) \tag{1.22}$$

where P_k is the tunneling probability for the kth time the particle hits the barrier (or barriers if there is more than one decay channel, as for the potential well in Fig. 1), and $K(t)$ is the number of hits that have occurred by time t. Eq. (1.22) states that the net probability of not having tunneled out by time t is the probability of not tunneling out each time the particle hits the barrier.

The survival probability of Eq. (1.22) is for a single trajectory, and this must therefore be averaged over an appropriate distribution of trajectories (i.e., initial conditions). This averaging procedure is described in detail in section I.D.2. Such an averaged survival probability $\langle P_s(t) \rangle$ should decay exponentially, and the unimolecular rate constant k is obtained as the negative slope of a plot of $\ln \langle P_s(t) \rangle$ versus t.

For small tunneling probabilities, i.e., $P_k \ll 1$, Eq. (1.22) is difficult to evaluate directly (because, for example, $1 - 10^{-14} \simeq 1$ on a computer), so it is useful to compute first the cummulative tunneling probability $P_{tun}(t)$:

$$P_{tun}(t) \equiv 1 - P_s(t) \tag{1.23}$$

which can be shown to be given by

$$P_{tun}(t) = \sum_{k=1}^{K(t)} P_k(1-P_{k-1})(1-P_{k-2}) \cdots (1-P_2)(1-P_1) \qquad (1.24)$$

In this expression, if $P_k << 1$, then the cummulative tunneling probability simplifies to

$$P_{tun}(t) \simeq \sum_{k=1}^{K(t)} P_k \qquad (1.25)$$

and this causes no computational difficulty. This quantity is then averaged over appropriate initial conditions (see section I.D.2) to give $\langle P_{tun}(t) \rangle$, and then the averaged survival probability is obtained simply by

$$\langle P_s(t) \rangle = 1 - \langle P_{tun}(t) \rangle \qquad (1.26)$$

The key to this probability branching model is how the tunneling probabilities P_k are computed. The most rigorous semi-classical approach[30] would be to integrate the classical equations of motion along the complex time contours for which the particle tunnels through the barrier. Such an approach, however, is known to be very difficult to apply in practice, largely due to instabilities which arise in the propagation of the complex valued trajectories.[31] Approximate versions of this rigorous approach based on the assumption of

vibrationally adiabatic motion through the barrier are much simpler to implement, and in the calculations presented in section I.D.3 , the simplest of these approximations is used, i.e., the vibrationally adiabatic zero curvature (VAZC) approximation.[32] Other forms of vibrationally adiabatic approximations were attempted (e.g., the Marcus-Coltrin approximation[32b]), but results showed little or no sensitivity to the level of vibrationally adiabatic approximation used.

Within the VAZC approximation, the classical Hamiltonian used to describe the tunneling is

$$H(p_s,s,n) = \frac{p_s^2}{2m} + V_o(s) + (n + \tfrac{1}{2})\,\hbar\omega(s) \qquad (1.27)$$

where s is the reaction coordinate (the steepest descent path down from the saddle point), n is the vibrational action variable (i.e., the quantum number analogue) for the transverse vibration, $V_o(s)$ is the potential energy along the reaction coordinate, and $\omega(s)$ is the transverse vibrational frequency, which is a function of the reaction coordinate (thus maintaining the effects due to frequency modulation). The classical trajectories for intramolecular motion are computed using the full classical Hamiltonian in Eq. (1.5), the approximate Hamiltonian of Eq. (1.27) being used only for the purpose of determining an approximate tunneling probability for the branching model. At time t_k , the kth turning point for motion along the s direction, the current value of the vibrational action

variable n_k is determined by energy conservation and Eq. (1.27) :

$$n_k = \left. \frac{E - V_o(s)}{\hbar\omega(s)} \right|_{s=s(t_k)} - \frac{1}{2} \qquad (1.28)$$

The tunneling probability is then given within the VAZC approximation by the semi-classical tunneling expression[33]

$$P_k = e^{-2\theta_k} / (1 + e^{-2\theta_k}) \qquad (1.29)$$

where

$$\theta_k = \int_{s_<}^{s_>} ds \sqrt{2m(V_{eff}(s) - E)} \qquad (1.30a)$$

$$V_{eff}(s) = V_o(s) + (n + \frac{1}{2}) \hbar\omega(s) \qquad (1.30b)$$

2. Initial Conditions

In order to make the connection to the quantum mechanical decay rates, it is necessary to choose initial conditions which most closely correspond to state specific preparation, i.e., the metastable states. This is accomplished by computing the survival probability, and thus the unimolecular rate constant, corresponding to a definite total energy E and a specific initial value for n_v , the zeroth

order quantum number for the bound degree of freedom. Since n_y is only an approximate quantum number for the coupled system, this type of mode specific preparation of the system is not precisely equivalent to that produced by the quantum calculations of section I.C , but is an approximate simulation of the true situation. Most important, for our purposes, it does give the same kind of information, i.e., how the rate for a given total energy varies if the energy is initially distributed in the molecule in various ways.

To specify the average over initial conditions corresponding to a given energy E and initial n_y , it is convenient to specify the bound coordinate and momentum (y , p_y) in terms of their harmonic action angle variables[34]

$$y = \sqrt{\frac{(2n_y + 1)\hbar}{m\omega_y}} \sin q_{n_y} \qquad (1.31a)$$

$$p_y = \sqrt{(2n_y + 1)\hbar m\omega_y} \cos q_{n_y} \qquad (1.31b)$$

For state specific preparation, n_y is set initially to an integer (the initial vibrational quantum number for the bound oscillator) and q_{n_y} is to be averaged over. The average over q_{n_y} is carried out by standard Monte Carlo methods,[26] i.e., q_{n_y} is chosen as $2\pi\xi_i$ for the ith trajectory, where ξ_i is a random number uniformly chosen in the interval (0 , 1) .

The x motion is always started at a classical turning point $x_>$ defined by the condition $p_x = 0$, with $x_>$ being determined from energy conservation

$$H (p_x = 0 , p_y, x_>, y) = E \tag{1.32}$$

The average over the phase of the x motion is effected by averaging over time t for the first period of x oscillation. To see how this is accomplished, consider the function $P^{(i)}_{tun}(t)$, the function $P_{tun}(t)$ of Eq. (1.24) for the ith trajectory whose initial conditions are given by

$$q_{n_y} = 2\pi\xi_i \tag{1.33a}$$

$$n_y = \text{given integer} \tag{1.33b}$$

$$p_x = 0 \tag{1.33c}$$

$$x = x_> \quad \text{(from Eq. (1.32))} \tag{1.33d}$$

Let $\{ t^{(i)}_k \}$ and $\{ P^{(i)}_k \}$, k=1,2, ··· denote the times of the x turning points and the tunneling probabilities at these times, respectively. Fig. 10a sketches the typical form of $P^{(i)}_{tun}(t)$. The explicit expression for $P^{(i)}_{tun}(t)$ is

$$P^{(i)}_{tun}(t) = \sum_{k=1}^{\infty} P^{(i)}_k \, h(t-t^{(i)}_k) \tag{1.34}$$

where the quantity $P_k^{(i)}$ is defined by

$$P_k^{(i)} \equiv P_k^{(i)} (1-P_{k-1}^{(i)})(1-P_{k-2}^{(i)}) \cdots (1-P_2^{(i)})(1-P_1^{(i)}) \quad (1.35)$$

and h is the unit step function

$$h(x) = \begin{cases} 1 , & x > 0 \\ 0 , & x < 0 \end{cases} \quad (1.36)$$

Combining the time average and the Monte Carlo average over transverse vibrational phse yields the desired averaged tunneling probability

$$\langle P_{tun}(t) \rangle_{E,n_y} \equiv \frac{1}{N} \sum_{i=1}^{N} \frac{1}{t_1^{(i)}} \int_0^{t_1^{(i)}} dt' \, P_{tun}^{(i)}(t+t') \quad (1.37)$$

where N is the number of trajectories run (i.e., the number of Monte Carlo selections of q_{n_y}). The time average in Eq. (1.37) can be carried out explicitly by introducing the following function

$$Q_k^{(i)}(t) \equiv \frac{1}{t_1^{(i)}} \int_0^{t_1^{(i)}} dt' \, h(t + t' - t_k^{(i)}) \quad (1.38a)$$

$$= \begin{cases} 0 , & t < t_k^{(i)} - t_1^{(i)} \\ 1 + (t - t_k^{(i)})/t_1^{(i)} , & t_k^{(i)} - t_1^{(i)} < t < t_k^{(i)} \\ 1 , & t > t_k^{(i)} \end{cases} \qquad (1.38b)$$

so that the averaged tunneling probability is given finally by

$$\langle P_{tun}(t) \rangle_{E,n_y} = \frac{1}{N} \sum_{i=1}^{N} \sum_{k=-}^{\infty} P_{\kappa}^{(i)} Q_k^{(i)}(t) \qquad (1.39)$$

As previously described, Eq. (1.26) then gives the averaged survival probability for this mode specific preparation

$$\langle P_S(t) \rangle_{E,n_y} = 1 - \langle P_{tun}(t) \rangle_{E,n_y} \qquad (1.40)$$

the exponential decay of which gives the state specific rate constants $k_{n_y}(E)$.

Though this model has been developed so as to treat classically forbidden unimolecular decay processes, it is easy to show that these same equations reduce to the standard classical prescription[35] for computing the survival probability when the total energy is above the top of the classical barrier height. This is accomplished by setting the tunneling probabilities P_k to either 0 or 1 (depending on whether or not the classical motion passes over the barrier). One

needs only to note the time $t(i)$ at which trajectory i passes over the barrier, and the above equations reduce to

$$\langle P_{tun}(t) \rangle_{E,n_y} = \frac{1}{N} \sum_{i=1}^{N} Q^{(i)}(t) \qquad (1.41)$$

where

$$Q^{(i)}(t) \equiv \frac{1}{t_1^{(i)}} \int_0^{t_1^{(i)}} dt' \, h(t + t' - t^{(i)}) \qquad (1.42a)$$

$$= \begin{cases} 0 & t < t^{(i)} - t_1^{(i)} \\ 1 + (t - t^{(i)})/t_1^{(i)} , & t^{(i)} - t_1^{(i)} < t < t^{(i)} \\ 1 & t > t^{(i)} \end{cases} \qquad (1.42b)$$

Here, as before, $t_1^{(i)}$ is the time for the first oscillation in the x potential well.

3. Results and Observations

An illustration of the typical exponential decay of the survival probability, from which the rate constant k is obtained, is shown in Fig. 10b. For the separable case (Fig. 2), the VAZC approximation for the tunneling probability is essentially exact, and the classical (plus tunneling) rate constants are in excellent agreement

(within 10%) with the quantum results. Fig. 11 shows a typical comparison when there is coupling between the modes. The points are the quantum results from Fig. 7, which show a high degree of statistical character. The solid curves are the results of the classical model, plotted as a continuous function of E (i.e., no attempt was made to quantize the x-mode semi-classically).

An interesting feature of this classical model for unimolecular decomposition is that it enables one to investigate the effects of the classical motion more directly than from the quantum mechanical perspective. Consider, therefore, a trajectory initiated in the way prescribed in section I.D.2 , which is quasi-periodic in its motion. Due to its quasi-periodicity, the region of the total energy-allowed phase space (or configuration space) covered by this trajectory will be restricted. As a consequence, the region of the barrier which it hits as it oscillates back and forth will also be restricted more than if the trajectory were chaotic. The average of the tunneling probabilities within this restricted hitting region will be different than the average of the tunneling probabilities for other types of trajectories, thus giving rise to mode specific behavior as a consequence. Extension of this reasoning to the case of chaotic trajectories, however, is not straightforward due to the competing effects of intramolecular relaxation and unimolecular reaction, as discussed in section I.A .

In any event, the classical (plus tunneling) model yields rates in very reasonable agreement with the quantum values, even with the

relatively primitive VAZC approximation for the tunneling probabilities. Therefore, it seems plausible that this model (which is no more difficult to implement than standard classical trajectory methods) can be applied with success to more realistic polyatomic unimolecular systems.

II. The Henon-Heiles Potential Energy Surface

There have been a number of theoretical studies[11] on the classical intramolecular dynamics of model systems, such as those described in section I . A particularly striking feature of these studies is the existence of classical motion which is quasi-periodic at low energies, but which becomes ergodic (or stochastic) at higher energies. A mathematical theorem of non-linear dynamics, the KAM theorem[36], attempts to relate this transition in the intramolecular motion to the properties of the system, e.g., the potential. Many such related topics are currently being investigated[37] in the mathematics and physics communities.

Another question which has spurred much interest among many chemical dynamicists[38] concerns the correspondence between classical ergodicity and quantum ergodicity. Since non-linear systems of chemical interest (e.g., polyatomic molecules) actually obey quantum mechanics, it would be interesting to discover whether such a correspondence indeed exists, and if so how it is manifest in the quantum mechanical description. At present, many quantum mechanical features have been considered as probes of this correspondence, including the sensitivity of individual energy levels to small perturbations of the potential[38a], the "localized" or "extended" distribution of coefficients of basis functions used to expand the wave function[38b], the nodal patterns of the wave functions[38c], the overlap of true wave-

functions with degenerate subspaces corresponding to separable Hamiltonians[38d], etc. All of these approaches do indeed show quantum mechanical features which qualitatively correlate with the quasi-periodic/ergodic character of the classical mechanics.

Of central importance to the work at hand, however, is how these approaches relating to intramolecular relaxation bear on the question of mode specificity in unimolecular reaction dynamics. A naive expectation would be that quasi-periodic classical motion would lead to mode specific behavior of the rate constants and that ergodic-like classical motion would correlate with statistical behavior of the rates. As shown in the results of section I.C , however, very little correlation of this kind was observed for the model systems studied. For some potential surfaces for which the classical motion was quasi-periodic (see Figs. 2-8, section I.C.2), the rate constants showed strong mode specificity, and for others they did not.

To pursue further this question of the correlation between the quasi-periodic/ergodic classical behavior and the mode specific/statistical behavior of the unimolecular rate constants, a well-characterized system, the Henon-Heiles potential energy surface[39], was investigated. This model system consists of two coupled oscillators (as do the systems considered in section I.C), and it possesses three barriers to dissociation. At low energies, the classical motion is quasi-periodic, but at higher energies it becomes chaotic, these two regimes being separated by a strikingly sharp critical energy, E_c,

which lies slightly more than half way up to the barrier height. The aim, therefore, is to determine whether the quantum mechanical decay rates exhibit any sort of transition from mode specific character to statistical character, analagous to the classical motion.

A. Quantum Mechanical Calculations

The quantum mechanical Hamiltonian for the Henon-Heiles system has the following form:

$$H = \frac{-\hbar^2}{2m}\left(\frac{\partial^2}{\partial x^2} + \frac{\partial^2}{\partial y^2}\right) + \frac{1}{2} m \omega^2 \left(x^2 + y^2\right)$$

$$+ \lambda \left(-\frac{1}{3} x^3 + x y^2\right) \qquad (2.1)$$

Such a coupled oscillator system can be thought of as a collinear triatomic molecule in its center of mass frame. This Hamiltonian is transformed to a more standard form by introducing a reduced Planck's constant

$$\hbar' \equiv \frac{\hbar \lambda^2}{m^3 \omega^5} \qquad (2.2)$$

and a reduced energy unit

$$\varepsilon \equiv \frac{m^3 \omega^6}{\lambda^2} \qquad (2.3)$$

In these units, H becomes

$$H = \frac{-\hbar'^2}{2}\left(\frac{\partial^2}{\partial x^2} + \frac{\partial^2}{\partial y^2}\right) + \frac{1}{2}\left(x^2 + y^2\right)$$

$$- \frac{1}{3}x^3 + x y^2 \qquad (2.4)$$

in Cartesian coordinates. In polar coordinates (r, θ) , the potential energy has a form that more clearly depicts its C_{3v} symmetry,

$$V(r,\theta) = \frac{r^2}{2} - \frac{1}{3} r^3 \cos(3\theta) \qquad (2.5)$$

Note that this potential has three equivalent saddle points at the positions $(r,\theta) = (1,0)$, $(1, 2\pi/3)$, and $(1, 4\pi/3)$, with the value of the potential at the saddle points being $V_{sp} = 1/6$. For clarity in notation, $\hbar'$ will simply be referred to as $\hbar$, and by varying this parameter the system will become more or less quantum-like (i.e., large $\hbar$ is more quantum-like, small $\hbar$ is closer to the classical limit).

The classical mechanical investigations[11] of the Henon-Heiles system demonstrate that for energies below a critical value $E_c \simeq 0.11$, all trajectories are quasi-periodic, but above this value an increasingly large fraction of initial conditions in phase space leads to ergodic type trajectories. Very near to the classical barrier height,

essentially all phase space points give rise to ergodic trajectories. (This is not true in general, as demonstrated by studies of Hase, et al[40].)

Though no classical trajectories can ever dissociate for energies below V_{sp}, quantum mechanically the system has no bound states, there being only metastable states that decay by tunneling through the barriers. As for the model systems of section I.B, the complex scaling method[17] (see section I.C.1) was used to calculate the complex eigenvalues corresponding to these metastable states.

The C_{3v} symmetry of the Henon-Heiles potential gives rise to states corresponding to different irreducible representations, A_1, A_2, and E. The basis set used for expanding the scaled Hamiltonian was of the form (in polar coordinates)

$$\phi_{n,m}(r,\theta) = r^n \exp\{-\alpha_n r^2/2\} e^{im\theta} \qquad (2.6)$$

which is similar, but not identical, to the standard two dimensional harmonic oscillator basis[41]. The exponential coefficients, α_n, allow for extra diffuseness for large values of n, enabling the calculations to be stable using smaller basis set expansions.

For this basis set, the three irreducible representations correspond to the following grouping of functions:

$$A_1 : \quad \cos(m\theta) \quad , \quad m = 0, 3, 6, \cdots \quad m \leq n \qquad (2.7a)$$

$$A_2 : \quad \sin(m\theta) \quad , \quad m = 3, 6, 9, \cdots \quad , \quad m \leq n \qquad (2.7b)$$

$$E : \quad e^{im\theta} \quad , \quad m = \begin{cases} \cdots, -5, -2, 1, 4, \cdots \\ \cdots, -4, -1, 2, 5, \cdots \end{cases} , \qquad (2.7c)$$

$$|m| \leq n$$

where the two groups of m values for the E states give rise to the double degeneracy of these states.

In polar coordinates, the radial coordinate must be scaled as

$$r \rightarrow re^{i\beta}$$

and the angle θ remains real. The transformed Hamiltonian H has the form

$$H_\beta = e^{-2i\beta}\left(-\frac{\hbar^2}{2}\right)\left(\frac{\partial^2}{\partial r^2} + \frac{1}{r}\frac{\partial}{\partial r} + \frac{1}{r^2}\frac{\partial^2}{\partial \theta^2}\right)$$

$$+ e^{2i\beta} r^2/2 - e^{3i\beta} r^3/3 \cos(3\theta) \qquad (2.8)$$

which is to be expanded in the irreducible representation basis sets of Eq. (2.7) and diagonalized.

Figs. 12, 13, and 14 show the unimolecular decay rates versus energy for values of $\hbar$ = 0.04, 0.03, and 0.02, respectively. The value of $\hbar$ is chosen to make the system more (larger $\hbar$) or less (smaller $\hbar$) quantum-like, and to speed up or slow down the tunneling rates. The number of states up to energy E for two degenerate har-

monic oscillators is[42]

$$N(E) = \frac{1}{2} (E/\hbar)^2 \tag{2.9}$$

and so the approximate number of states in the Henon-Heiles systems up to the energy of the saddle point (1/6) is

$$N_b \simeq \left(\frac{1}{72\ \hbar^2} \right) \tag{2.10}$$

A value of $\hbar = 0.04$ (see Fig. 12) thus produces about nine classically bound states, and a value $\hbar = 0.02$ leads to about 35 classically bound states. Since the larger the number of states to be obtained requires larger basis set expansions, the value $\hbar = 0.02$ represents a practical limit for the present problem in obtaining satisfactory quantum mechanical results. Indeed, for the case $\hbar = 0.02$ only the A_1 and A_2 states could be obtained, the E state basis set being about twice as large and computationally intractable.

B. Observations

1. Symmetry-induced Mode Specificity

A particularly striking feature of Figs. 12-14 is that the A_1 and E type of states display significantly different rate profiles than the A_2 states. More specifically, for a given energy, the A_2 states decay more slowly than the A_1 and E states. This symmetry-induced more specificity is readily understood by realizing that A_2

states have a nodal line from the origin through each saddle point (due to the factor $\sin(m\theta)$, $m = 3, 6, \ldots$, in the wavefunctions for A_2 states, Eq. (2.7b)). This means that the vibrational states of the "activated complex" (i.e., the local vibrational modes at the saddle points of the potential energy surface) must be odd.

The microcanonical transition state theory rate constant expression (i.e., the RRKM rate expression), including tunneling,[15] is

$$k(E) = 3 \times \{2\pi\hbar\rho(E)\}^{-1} \sum_{n=0} P\{E-(n + \tfrac{1}{2})\hbar\omega^{\ddagger}\} \qquad (2.11)$$

where $\rho(E)$ is the density of states of the reactants at energy E, and $P(E_t)$ is the tunneling probability with energy $E_t = E - (n + \frac{1}{2})\hbar\omega^{\ddagger}$ in the reaction coordinate direction. The factor of three is due to the three equivalent saddle points of the Henon-Heiles potential surface.

In the tunneling region, where only the lowest state in the sum in Eq. (2.11) contributes significantly to the rate, transition state theory implies that

$$k_{A_1}(E) \simeq (\text{frequency factor}) \times P(E - \tfrac{1}{2}\hbar\omega^{\ddagger}) \qquad (2.12a)$$

$$k_{A_2}(E) \simeq (\text{frequency factor}) \times P(E - \tfrac{3}{2}\hbar\omega^{\ddagger}) \qquad (2.12b)$$

where P is the one-dimensional tunneling probability. This is due to the fact that the A_2 states must be odd with respect to reflec-

tion across the reaction coordinate, and the lowest state of this symmetry contributing to the sum in Eq. (2.11) is the state for which $n = 1$. This implies that

$$k_{A_2}(E) \simeq k_{A_1}(E - \hbar\omega^{\ddagger}) \tag{2.13}$$

where $\omega^{\ddagger}$ is the vibrational frequency at the saddle point for the transverse mode. For the Henon-Heiles surface,

$$\omega^{\ddagger} = \sqrt{3} \tag{2.14}$$

and Figs. 12-14 do indeed show that the rate constants for the A_1 and A_2 states are displaced in energy by approximately $\hbar\omega^{\ddagger} = \sqrt{3}\,\hbar$.

2. The Classical Limit

Within a given irreducible representation, the rate constants show essentially no mode specificity, i.e., within each symmetry class the rate constants appear to be a smooth function only of the total energy. For these systems, the striking classical transition from quasi-periodic to ergodic behavior at the energy $E_c \simeq 0.11$ is not observed. In fact, only among the E states is there any hint of mode specificity, and this only occurs at higher energies.

To verify whether the rate constants obtained from the quantum mechanical calculations correspond to the statistical rates more

quantitatively, the RRKM plus tunneling model[15] was used. This model has been used for several molecular systems of physical interest in attempting to ascertain the importance of tunneling in certain unimolecular reactions.[43] The density of states $\rho(E)$ in Eq. (2.11) is

$$\rho(E) = E/\hbar^2 \tag{2.15}$$

and the one dimensional tunneling probability P is given semi-classically[33] by

$$P(E_t) = (1 + e^{2\theta(E_t)})^{-1} \tag{2.16a}$$

$$\theta(E_t) = \frac{1}{\hbar} \int_{x_<}^{x_>} dx \sqrt{2(V(x) - E_t)} \tag{2.16b}$$

$$V(x) = x^2/2 - x^3/3 \tag{2.16c}$$

The barrier penetration integral $\theta(E_t)$ is well approximated for this cubic barrier case by

$$\theta(E_t) \simeq \frac{\pi}{\hbar} \{(\frac{1}{6} - E_t) + \frac{5}{12}(\frac{1}{6} - E_t)^2 + \frac{385}{432}(\frac{1}{6} - E_t)^3\} \tag{2.17}$$

The solid curves in Figs. 12-14 show that the rates of the A_1 and E states are reasonably well described within this simple statistical model, i.e., even the individual metastable states of these two sym-

metries have coalesced to the statistical limit. The fact that the A_2 states decay more slowly at a given energy could be described by the statistical model by excluding the even vibrational states in the sum in Eq. (2.11) from the activated complex.

Though the results shown in Figs. 12-14 are the essentially exact results for these values of $\hbar$, there is still one final question which must be resolved before any conclusions about the classical/quantum mechanical correspondence can be made. It is possible that we have not allowed $\hbar$ to become sufficiently small for any underlying classical structure to emerge in the quantum rate constants. The purely classical limit ($\hbar \to 0$) is far beyond the reach of the quantum mechanical approach employed here.

It is possible to extrapolate to the classical limit ($\hbar \to 0$), however, by noting that in the form for the statistical rate constant

$$k(E) \simeq \text{(frequency factor) x (tunneling probability)} \quad (2.18)$$

the frequency factor has a classical limit which is independent of $\hbar$. The tunneling probability has the limiting form (semi-classically)

$$\text{tunneling probability} \simeq \exp\{ -2\theta(E)/\hbar \} \quad (2.19)$$

where $\theta(E)$ is the classical action integral given for the Henon-Heiles system by Eqs. (2.16) and (2.17). These facts imply that the quantity

$$\hbar \ln k(E)$$

should have a classical limit given by

$$\lim_{\hbar \to 0} \hbar \ln k(E) = -2\,\theta(E) \tag{2.20a}$$

or

$$\lim_{\hbar \to 0} \hbar \log k(E) = -2\,\theta(E) \log e \simeq -0.87\,\theta(E) \tag{2.20b}$$

Figs. 15 and 16 show the quantity $\hbar \log k(E)$ for $\hbar = 0.02$, 0.03, and 0.04, for the A_1 and the A_2 states, respectively. Also shown is the RRKM plus tunneling approximation to the classical limit of this quantity, Eq. 2.20b. It appears that (1) the quantum rate constants are approaching the $\hbar \to 0$ limit in a smooth manner with no evidence of any new classical structure emerging, (2) the simple RRKM plus tunneling model is a reasonably good approximation to the $\hbar \to 0$ limit of the quantum rate constants, and (3) both the A_1 and A_2 states converge to the same $\hbar \to 0$ limit (as is implied by the approximate relation in Eq. (2.12)).

C. A One-barrier Henon-Heiles Potential

The existence of three equivalent barriers to dissociation for the Henon-Heiles potential in Eq. (2.5) precludes the possibility of energy being trapped in a mode which does not significantly project

onto one of the dissociative channels, even for energies where the classical motion is completely quasi-periodic. To test whether this effect might be responsible for the lack of mode specificity for the Henon-Heiles surface, similar calculations were carried out for a one-barrier Henon-Heiles-like potential energy surface,

$$V(r,\theta) = \frac{1}{2} r^2 - \frac{1}{3} r^3 \cos\theta \qquad (2.21a)$$

$$= \frac{1}{2}(x^2 + y^2) - \frac{1}{3} x^3 - \frac{1}{3} x y^2 \qquad (2.21b)$$

The one saddle point for this system occurs at $(r,\theta) = (1,0)$ and the barrier height is still $V_{sp} = 1/6$.

For this system, the states divide into two symmetry classes, even and odd with respect to reflection about the x-axis. Fig. 17 shows the unimolecular rate constants as a function of energy (obtained by the complex scaling method) for $\hbar = 0.03$. As opposed to the three barrier case of section II.B , there is substantial mode specificity even within the same irreducible representation.

The classical behavior for the one-barrier Henon-Heiles system was studied by generating the Poincare surfaces of section[25] for several energies. This system possesses only quasi-periodic trajectories for all energies up to the top of the barrier.

This potential surface, therefore, does show the expected correlation, i.e., the classical mechanics is quasi-periodic for all energies (below the top of the barrier), and the quantum mechanical unimolecular decay rates are highly mode specific. No conclusions can be drawn,

however, with respect to the statistical/chaotic correlation or the transition from one type of motion to the other.

D. Discussion

It appears, based on the results of sections I.C and II.B, C that there is not necessarily a correlation between the quasi-periodic/ergodic classical behavior and the mode specific/statistical behavior in quantum mechanical decay rates for unimolecular systems. Some examples seem to show a correlation (see section II.C) while others tend to show no correlation (see section I.C) .

Since many of the studies in intramolecular dynamics relating classical and quantum features[38] do succeed in showing a qualitative correspondence (e.g., in nodal patterns of wave functions, etc.), it seems unlikely that the lack of correlation spoken of in the preceding paragraph should be due to a quantum/classical non-correspondence of some sort. Rather, it seems clear that the two approaches taken are in fact monitoring different phenomena, and therefore need not show any particular correlation, as discussed in detail in section I.B .

Another relevant factor, illustrated by the examples of the Henon-Heiles and one-barrier Henon-Heiles systems, is the coupling of the intramolecular motion to the reaction product channels. It seems clear that mode specific reaction dynamics requires not only mode specific (i.e., quasi-periodic) intramolecular dynamics but also mode specific coupling to the reaction products. For the three barrier

Henon-Heiles system, the three exit valleys effectively provide statistica'-like coupling to products since there is no mode (i.e., direction ı the x-y plane) which does not project significantly onto a reaction coordinate for at least one of the exit valleys. The one-barrier He on-Heiles system, however, does possess a mode (e.g., motion in he y direction) which effectively avoids the saddle point leading to dissociation.

III. A Semi-classical Multi-channel Branching Model

Quantum mechanical calculations such as those presented in sections I and II are the rigorously correct way to characterize state-specific unimolecular decay. Unfortunately, however, such an approach is not feasible for systems with more than two or three degrees of freedom. For example, the unimolecular decomposition of formaldehyde

$$H_2CO \rightarrow H_2 + CO \tag{3.1}$$

has six vibrational degrees of freedom (we are ignoring rotations for the present) and is thus beyond the capabilities of these rigorous quantum mechanical approaches.

As discussed in section I.D, an alternate approach to the characterization of state specific unimolecular decay is the use of classical mechanics, via either the straightforward trajectory simulation approach[26] or an approach, as in section I.D, incorporating such quantum features as tunneling. There have been many such calculations for unimolecular systems[27], and in many situations such an approach has been shown to describe the process correctly. For the example of Eq. (3.1), however, the energy region where the reaction proceeds may involve tunneling[28,29] and a standard classical approach would be [illegible] in section I.D.

Furthermore, there may be cases for which the unimolecular decay, though energetically possible classically, simply does not take place via classical mechanics. Hase[40], for example, has observed quasi-periodic trajectories which have enough energy to dissociate classically but which do not for some unimolecular systems. Heller[44] has discussed such dynamically forbidden processes under the term "dynamic tunneling." Simple classical mechanics would give zero for the rate of unimolecular decomposition for such a system, whereas the true (quantum mechanical) rate in non-zero.

The classical trajectory (plus tunneling) approach of section I.D provides one way of qualitatively characterizing the mode specificity of unimolecular reactions. However, even this approach is not capable of reliably determining state-specific decay rates, due to the difficulties associated with quantization of non-separable systems.[45] Yet there are situations for which a quantum mechanical description of the unimolecular decay rates will be necessary. Therefore, the purpose of this section is to describe and illustrate an approximate quantum mechanical model for determining state-specific unimolecular decay rates, one which is capable of being applied to polyatomic molecular systems of interest, such as the formaldehyde system of Eq. (3.1).

The model to be presented is related to several methods developed in recent years, as well as to several old ideas. First, it is a multi-channel version of a semi-classical branching model that has been shown to describe unimolecular decay in one-dimensional systems cor-

rectly.[46] The multi-channel aspect of the model is what enables it to be applicable to systems consisting of several degrees of freedom. The dynamical approximations incorporated in the model include the reaction path Hamiltonian of Miller, Handy, and Adams[47] and a semi-classical perturbation-infinite order sudden approximation developed by Miller and Shi.[48] The reaction path model describes the molecular dynamics as motion along a reaction coordinate which is coupled to transverse locally harmonic vibrational modes. The semi-classical perturbation-infinite order sudden approximation (SCP-IOS) allows for vibrational inelasticity in the transverse vibrational modes as the system moves along the reaction coordinate.

A. General Development of the S-Matrix

Instead of considering the unimolecular decomposition in terms of the out-going wave boundary conditions (i.e., the half-collision process) of section I.C, the multi-channel branching model is developed in terms of an overall scattering matrix, the poles of which will correspond to the energies of the metastable states associated with the system.[13] Consider, therefore, the nonreactive scattering on a potential energy surface for which the potential energy along the reaction coordinate s is as depicted in Fig. 18. For such a scattering process, the system begins as $s = +\infty$, moves to the left, collides, and eventually returns to $s = +\infty$. If there are F total number of degrees of freedom, there are $F - 1$ vibrational degrees of freedom orthogonal to the reaction coordinate (we shall neglect rotations for the present).

The aim of this development is to construct an approximate S-matrix for the total energy E,

$$\underset{\sim}{S}(E) = \{ S_{\underset{\sim}{n},\underset{\sim}{n}'} \} \tag{3.2}$$

which are the amplitudes for transitions between an initial state $\underset{\sim}{n} = (n_1, n_2, \ldots n_{F-1})$, and a final state $\underset{\sim}{n}' = (n_1', n_2', \ldots n_{F-1}')$ of the transverse vibrational modes at $s = +\infty$. The central idea of the branching model is to approximate this net amplitude $\underset{\sim}{S}$ as a sum of amplitudes constructed from the different "trajectories" which can arise from tunneling through the barrier in Fig. 18. The most straightforward way to construct these "amplitude trajectories" is demonstrated in Fig. 19, where the first three are depicted. The first is reflected by the barrier (at the classical turning point, say) without tunneling, the second tunnels through and makes one oscillation in the well before tunneling back out, the third tunnels through and makes two oscillations in the well before tunneling back out, and so on. The amplitude associated with first "trajectory" is

$$\underset{\sim}{S}_{out} \cdot (\underset{\sim}{1} - \underset{\sim}{P})^{1/2} \cdot \underset{\sim}{S}_{in} \quad , \tag{3.3a}$$

that associated with the second "trajectory" is

$$\underset{\sim}{S}_{out} \cdot \underset{\sim}{P}^{1/2} \cdot \underset{\sim}{S}_{o} \cdot \underset{\sim}{P}^{1/2} \cdot \underset{\sim}{S}_{in} \tag{3.3b}$$

and that with the third trajectory is

$$(-1)\,\underset{\sim}{S}_{out}\cdot\underset{\sim}{P}^{1/2}\cdot\underset{\sim}{S}_{o}\cdot(\underset{\sim}{1}-\underset{\sim}{P})^{1/2}\cdot\underset{\sim}{S}_{o}\cdot\underset{\sim}{P}^{1/2}\cdot\underset{\sim}{S}_{in} \qquad (3.3c)$$

and so on. In these expressions, $\underset{\sim}{S}_{in}$ is the S-matrix (i.e., matrix of transition amplitudes) associated with the incoming motion from $s = +\infty$ to the outer turning point $s = s_3$ (see Fig. 18). $\underset{\sim}{S}_{o}$ is the S-matrix for the motion in the interior well from $s = s_2$ to s_1 and back to s_2. And $\underset{\sim}{S}_{out}$ is the S-matrix for the outgoing motion from $s = s_3$ back to $+\infty$. $\underset{\sim}{P}$ is the matrix of tunneling probabilities (i.e., $\underset{\sim}{P}^{1/2}$ is a tunneling amplitude matrix, and $(\underset{\sim}{1}-\underset{\sim}{P})^{1/2}$ is a reflection amplitude matrix). Note that $\underset{\sim}{S}_{in}$ and $\underset{\sim}{S}_{out}$ are in general rectangular matrices since there are in general a different number of transverse vibrational states that are energetically open at $s = s_3$ and $s = +\infty$. Thus, in the matrix element $S^{(in)}_{\underset{\sim}{n},\underset{\sim}{n}'}$, for example, $\underset{\sim}{n}'$ refers to transverse vibrational states at $s = +\infty$ and $\underset{\sim}{n}$ to those at $s = s_3$, while for $S^{(out)}_{\underset{\sim}{n},\underset{\sim}{n}'}$ the identifications are reversed. (By symmetry, in fact, $\underset{\sim}{S}_{out}$ is the transpose of $\underset{\sim}{S}_{in}$.) $\underset{\sim}{S}_{o}$ is a square matrix, the indices of which refer to the transverse vibrational states at $s = s_2$. It is clear that the physical meaning of the matrices $\underset{\sim}{S}_{in}$ and $\underset{\sim}{S}_{out}$ is that they describe vibrational inelasticity in the region outside the barrier, whereas $\underset{\sim}{S}_{o}$, the S-matrix per oscillation in the well, describes vibrational inelasticity in the region of the potential well. Although it is not

necessary, the matrix $\underset{\sim}{P}$ is assumed to be square (i.e., the same number of vibrational states are open at $s = s_2$ and s_3), and for the applications presented in section III.D it is even approximated as diagonal (i.e., the tunneling proceeds adiabatically). All of the matrices are functions of the total energy E, i.e., $\underset{\sim}{S}_{in} = \underset{\sim}{S}_{in}(E)$, etc.

The net amplitude $\underset{\sim}{S}$ is obtained by adding the amplitudes for all the trajectories of the type described in Fig. 19, i.e.,

$$\underset{\sim}{S} = \underset{\sim}{S}_{out} \cdot \left(\underset{\sim}{1} - \underset{\sim}{P} \right)^{1/2} \cdot \underset{\sim}{S}_{in} + \sum_{k=0}^{\infty} (-1)^k \, \underset{\sim}{S}_{out} \cdot \underset{\sim}{P}^{1/2} \cdot \underset{\sim}{S}_{o} \cdot \left[\left(\underset{\sim}{1} - \underset{\sim}{P} \right)^{1/2} \underset{\sim}{S}_{o} \right]^k \cdot \underset{\sim}{P}^{1/2} \cdot \underset{\sim}{S}_{in} \tag{3.4}$$

The general kth term in Eq. (3.4) has the direct mechanistic interpretation by simply reading the various factors from right to left: the system evolves from $s = +\infty$ to s_3 ($\underset{\sim}{S}_{in}$), tunnels through the barrier ($\underset{\sim}{P}^{1/2}$) , oscillates in the well (k+1) times, not tunneling out each time it is reflected at s_2 ($(\underset{\sim}{1} - \underset{\sim}{P})^{1/2}$), tunnels out through the barrier ($\underset{\sim}{P}^{1/2}$) , and finally moves from s_3 back out to $s = +\infty$ ($\underset{\sim}{S}_{out}$). The factor $(-1)^k$ enters because of the extra reflections involved in the kth trajectory.

The geometric series in Eq. (3.4) is easily summed (remembering to keep track of the order of matrix multiplications) to yield

$$\underset{\sim}{S} = \underset{\sim}{S}_{out} \cdot \left(\underset{\sim}{1} - \underset{\sim}{P} \right)^{1/2} \cdot \underset{\sim}{S}_{in}$$

$$+ \underset{\sim}{S}_{out} \cdot \underset{\sim}{P}^{1/2} \cdot \underset{\sim}{S}_{o} \cdot \left[\underset{\sim}{1} + \left(\underset{\sim}{1} - \underset{\sim}{P} \right)^{1/2} \cdot \underset{\sim}{S}_{o} \right]^{-1} \cdot \underset{\sim}{P}^{1/2} \cdot \underset{\sim}{S}_{in} \qquad (3.5)$$

Eq. (3.5) is the general result for the S-matrix given by this semiclassical multichannel branching model, as applied to a scattering system such as depicted in Fig. 18. Applications to other types of scattering systems (see section III.E) are similar to the above development. The semi-classical aspect of the branching model is that we have used it to construct a probability amplitude. Other branching models have constructed probabilities,[49] and these would be referred to as classical branch models (see also section III.E.2). The multichannel aspect of the present model is that the quantities $\underset{\sim}{S}_{o}$, $\underset{\sim}{P}$, $\underset{\sim}{S}_{in}$, $\underset{\sim}{S}_{out}$ are matrices in the transverse vibrational states $\underset{\sim}{n} = (n_1, n_2, \ldots n_{F-1})$, and as such it is necessary to maintain the correct order of the matrix products in Eqs. (3.4) and (3.5). The matrix products, which involve sums over intermediate transverse vibrational states, are a manifestation of the quantum principle that one sums over all intermediate states that are not observed.[50]

B. Application to Unimolecular Decomposition

Though the general result of Eq. (3.5) gives the overall S-matrix for the collision process depicted in Fig. 18, it is also

possible to extract from the result information regarding the unimolecular decay of the system. The connection lies in considering the collision complex (i.e., when the system is in the well region of Fig. 18) to be a prepared unimolecular system, which reacts to yield products (i.e., goes to $s = +\infty$ in Fig. 18). As before, the individual metastable states are characterized by complex energy eigenvalues

$$E = E_r - i\,\Gamma / 2 \tag{3.6}$$

the real part of which is the energy of the state (E_r) and the imaginary part of which determines the width of the state, Γ (see Eq. (1.6)).

The complex eigenvalues of the metastable system (i.e., the collision complex) are defined rigorously[13] as the poles of the S-matrix $\underset{\sim}{S}(E)$. Therefore, the approximate full S-matrix of Eq. (3.5) is used to determine these poles. By inspection of the form for the scattering matrix, it is clear that poles of $\underset{\sim}{S}(E)$ occur at values of E for which the inverse matrix in the second term in Eq. (3.5) is singular, i.e., values of E for which

$$\det\left| \underset{\sim}{1} + \left[\underset{\sim}{1} - \underset{\sim}{P}(E) \right]^{1/2} \cdot \underset{\sim}{S}_o(E) \right| = 0 \tag{3.7}$$

where it is emphasized that $\underset{\sim}{P}$ and $\underset{\sim}{S}_o$ are functions of energy.

Eq. (3.7) essentially serves to quantize the quasi-bound states of the system, and hence is the desired equation for determining

the state specific energies and lifetimes of the metastable system. As one would expect, the equation involves only the interior S-matrix, $\underset{\sim}{S}_o$, and the tunneling probabilities, and not the exterior S-matrices $\underset{\sim}{S}_{in}$ and $\underset{\sim}{S}_{out}$. Of course, if one desired to determine product state distributions of unimolecular reactions, it would be necessary to include the effects from these external S-matrices via the full scattering S-matrix, Eq. (3.5).

In applying Eq. (3.7) to one-dimensional systems (i.e., no transverse vibrational modes), $\underset{\sim}{P}$ and $\underset{\sim}{S}_o$ become 1 x 1 matrices, i.e., simple numbers. The semi-classical (WKB) approximation[51] for them is

$$S_o(E) = e^{2i\phi(E)} \tag{3.8a}$$

$$P(E) = e^{-2\theta(E)}/(1 + e^{-2\theta(E)}) \tag{3.8b}$$

where $\phi(E)$ is the WKB phase integral across the well

$$\phi(E) = \frac{1}{\hbar} \int_{s_1}^{s_2} ds \sqrt{2(E - V(s))} \tag{3.9}$$

and $\theta(E)$ is the barrier penetration integral

$$\theta(E) = \frac{1}{\hbar} \int_{s_2}^{s_3} ds \sqrt{2(V(s) - E)} \tag{3.10}$$

The condition for determining the poles of the S-matrix then takes the form

$$1 + e^{2i\phi} / (1 + e^{-2\theta})^{1/2} = 0 \qquad (3.11)$$

which is equivalent to

$$\phi(E) = \left(n + \frac{1}{2} \right) \pi - \frac{i}{4} \ln \left(1 + e^{-2\theta} \right) \qquad (3.12)$$

In the tunneling region (i.e., when $e^{-2\theta} << 1$) the expression Eq. (3.12) can be expanded in a Taylor series about the real part of the complex energy, $E_r - i \Gamma / 2$, then equating real and imaginary parts. This gives the usual WKB eigenvalue equation for the real part of the complex energy

$$\phi(E_r) = \left(n + \frac{1}{2} \right) \pi \qquad (3.13)$$

and a width given by

$$\Gamma = (dE_r/dn)/2\pi \, e^{-2\theta} \qquad (3.14)$$

which is the well-known semiclassical result[46] for the one-dimensional case (dE_r/dn is the semiclassical expression for the frequency of oscillation in the well).

Finally, although the construction of the S-matrix in Eq. (3.5) has referred to the situation shown in Fig. 18, where there is an actual barrier to dissociation, this is not a necessary condition.

Suppose, for example, that the reaction coordinate profile of potential energy is actually a Morse potential:[52]

$$V_o(s) = D\left[e^{-2\alpha(s-s_o)} - 2\, e^{-\alpha(s-s_o)} \right] \tag{3.15}$$

For energy E the classical turning points, defined by $V_o(s) = E$, are

$$s = s_o - \frac{1}{\alpha} \ln \left(1 \pm \sqrt{1 + E/D} \right) \tag{3.16}$$

For $E < 0$ there are two real turning points, as expected, while for $E > 0$, the "+" sign in Eq. (3.16) gives the real inner turning point,

$$s_1 = s_o - \frac{1}{\alpha} \ln \left(1 + \sqrt{1 + E/D} \right) \tag{3.17}$$

and the "-" sign gives a complex outer turning point

$$s_2 = s_o - \frac{1}{\alpha} \ln \left(1 - \sqrt{1 + E/D} \right) \tag{3.18a}$$

or

$$s_2^{\pm} = s_o - \frac{1}{\alpha} \ln \left(\sqrt{1 + E/D} - 1 \right) \pm i\pi / \alpha \tag{3.18b}$$

The tunneling probability matrix $\underset{\sim}{P}$ for this situation will consist not of normal tunneling probabilities, but rather of transmission probabilities of passing into or out of the well from the outside (even though for real s there is no physical barrier that identifies the "inside" and "outside"). To be more specific, $\phi(\omega)$ in

Eq. (3.9) is replaced by

$$\frac{1}{\hbar}\int_{s_1}^{\mathrm{Re}\, s_2} ds\sqrt{2(E - V(s))}$$

and $\theta(E)$ in Eq. (3.10) is replaced by[33]

$$\frac{i}{\hbar}\int_{s_2^-}^{s_2^+} ds\,\left|\sqrt{2(E - V(s))}\right|$$

which is negative. For increasing energy above the barrier, the transmission probability (Eq. (3.8b)) approaches unity, i.e., the continuum limit, as indeed it must. This "above the barrier" situation is extended to the multi-channel case in the obvious straightforward manner, as discussed in section III.C.

C. Dynamical Approximations

The principle aim of the multi-channel branching model is to provide a quantum mechanical approach (though approximate) which can be applied to real polyatomic systems. It is therefore necessary to utilize relatively simple dynamical approximations in constructing the matrices $\underset{\sim}{S}_o$ and $\underset{\sim}{P}$ in Eq. (3.7). It should be emphasized that the Eqs. (3.4) and (3.5), describing the overall S-matrix, are general, and any one of a number of dynamical approximations could be implemented. The one chosen for this particular

study is the semi-classical perturbation-infinite order sudden approximation (SCP-IOS) discussed recently my Miller and Shi.[48]

The SCP-IOS approximation makes use of the reaction path Hamiltonian of Miller, Handy, and Adams[47] for modeling the molecular system. If (s, p_s) are the mass-weighted reaction coordinate and its conjugate momentum and $(\underset{\sim}{n}, \underset{\sim}{q}) \equiv (n_k , q_k)$, $k = 1, \ldots, F-1$ are the action-angle variables for the transverse vibrational modes, then the classical Hamiltonian has the form

$$H(p_s, s, \underset{\sim}{n}, \underset{\sim}{q}) = \frac{1}{2} \Big[p_s - \sum_{k,k'=1}^{F-1} B_{k,k'}(s) \sqrt{(2n_k+1)(2n_{k'}+1)} \times \sqrt{\omega_{k'}(s)/\omega_k(s)} \sin q_k \cos q_{k'} \Big]^2 \times \Big[1 + \sum_{k=1}^{F-1} B_{k,F}(s) \sqrt{(2n_k+1)/\omega_k(s)} \sin q_k \Big]^{-2} + V_o(s) + \sum_{k=1}^{F-1} (n_k + \tfrac{1}{2}) \omega_k(s) \qquad (3.19)$$

where $V_o(s)$ is the potential energy along the reaction path, $\omega_k(s)$ are the local harmonic frequencies of the transverse vibrational modes along the reaction path, and the matrix elements $B_{k,k'}(s)$ couple the transverse vibrational modes to each other and to the reaction coordinate (labeled as mode $k = F$). The manner in which this Hamiltonian is constructed from ab initio

quantum chemical calculations, and the nature of the coupling elements is described elsewhere.[43,47]

Since the action variables n_k are the classical counterpart of vibrational quantum numbers, this Hamiltonian provides a convenient framework for implementing the branching model as developed in section III.A .

Construction of the interior S-matrix, $\underset{\sim}{S}_o(E)$, within the SCP-IOS approximation is a relatively simple adaptation of the form for the scattering matrix given by Miller and Shi for scattering situations (the interior S-matrix is an amplitude transition matrix for one oscillation in the well). Employing units such that $\hbar = 1$, the expression for $\underset{\sim}{S}_o$ is

$$S_{\underset{\sim}{n},\underset{\sim}{n}'}(E) = \frac{e^{i\phi_o}}{(2\pi)^{F-1}} \int_0^{2\pi} d\underset{\sim}{q} \exp\left[-i\Delta\underset{\sim}{n}\cdot\underset{\sim}{q} + i\Delta\phi(\underset{\sim}{q})\right] \tag{3.20}$$

where $\Delta\underset{\sim}{n} = \underset{\sim}{n}' - \underset{\sim}{n}$ and

$$\phi_o = \phi_o(\underset{\sim}{n},E) = 2\int_{s_1}^{s_2} ds\sqrt{2(E - V_a(s))} \tag{3.21}$$

$$\Delta\phi(\underset{\sim}{q},\underset{\sim}{n},E) = \sum_{k=1}^{F-1} 2\sin q_k \int_{s_1}^{s_2} ds\,\sqrt{(E-V_a(s))}\,B_{k,F}(s)$$

$$\times \sqrt{(2n_k+1)/\omega_k(s)} \quad \cos \delta_k(s)$$

$$+ \sum_{k,k'=1}^{F-1} \Bigg\{ \cos(q_k - q_{k'}) \int_{s_1}^{s_2} ds\, B_{k,k'}(s) \sqrt{(2n_k+1)(2n_{k'}+1)}$$

$$\times \sqrt{\omega_{k'}/\omega_k} \sin(\delta_k - \delta_{k'})$$

$$+ \cos(q_k + q_{k'}) \int_{s_1}^{s_2} ds\, B_{k,k'}(s) \sqrt{(2n_k+1)(2n_{k'}+1)} \sqrt{\omega_{k'}/\omega_k}$$

$$\times \sin(\delta_k + \delta_{k'}) \Bigg\} \tag{3.22}$$

In Eqs. (3.20), (3.21), and (3.22), the term $\delta_k(s)$ is given by

$$\delta_k(s) = \int_{s_1}^{s_2} ds \frac{\omega_k(s)}{\sqrt{2(E - V_a(s))}} \tag{3.23}$$

The term $V_a(s)$ is the vibrationally adiabatic potential

$$V_a(s) = V_o(s) + \sum_{k=1}^{F-1} (n_k + \tfrac{1}{2})\, \omega_k(s) \tag{3.24}$$

and it is recognized that the quantum number index $\underset{\sim}{n}$ is to be replaced everywhere by the average of the initial and final quantum numbers,[53] i.e.,

$$\underset{\sim}{n} \rightarrow \frac{1}{2}\left(\underset{\sim}{n} + \underset{\sim}{n}'\right) \tag{3.25}$$

One recognizes the zeroth order phase of the above S-matrix, $p_o(E)$, as the vibrationally adiabatic WKB phase integral back and forth across the well. The phase term $\Delta\phi$ arises because of couplings between the various modes and thus gives rise to a non-diagonal S-matrix, i.e., to vibrational inelasticity. The central modification of the scattering situation expression for the S-matrix of Miller and Shi[48] lies in replacing the limits of integration corresponding to scattering conditions by the turning point limits of integration corresponding to the bounded motion inside the well.

The transition amplitude matrix, $\underset{\sim}{S}_o(E)$, is a probability conserving matrix, i.e., the system will be found in one of the transverse states $\underset{\sim}{n}$ both before and after the oscillation. Such a matrix is, by definition, a unitary matrix, i.e.,

$$\underset{\sim}{S}^{-} \cdot \underset{\sim}{S} = \underset{\sim}{S} \cdot \underset{\sim}{S}^{+} = \underset{\sim}{1} \tag{3.26}$$

The approximation to $\underset{\sim}{S}_o$ given by Eq. (3.20) however, will not be exactly unitary, and for the applications intended for this model this would cause serious errors. It becomes important, therefore, to unitarize the approximate matrix, $\underset{\sim}{S}_o$, in some fashion. Difficulties associated with unitarization have been encountered previously,[54] and various methods exist for unitarizing matrices. One way to accomplish this is via an R-matrix procedure.[55]

In general, an R-matrix and an S-matrix are related by

$$\underset{\sim}{S} = (\underset{\sim}{1} - i\underset{\sim}{R}) \cdot (\underset{\sim}{1} + i\underset{\sim}{R})^{-1} \tag{3.27a}$$

or inversely by

$$\underset{\sim}{R} = -i(\underset{\sim}{1} - \underset{\sim}{S}) \cdot (\underset{\sim}{1} + \underset{\sim}{S})^{-1} \tag{3.27b}$$

If $\underset{\sim}{S}$ is unitary, then $\underset{\sim}{R}$ is Hermitian, and vice versa. Thus, if $\underset{\sim}{S}$ is not unitary, then $\underset{\sim}{R}$ given by Eq. (3.27b) will not be Hermitian. One can make $\underset{\sim}{R}$ Hermitian, however, by simply taking its Hermitian part:

$$\underset{\sim}{R}_H = \frac{1}{2} (\underset{\sim}{R} + \underset{\sim}{R}^{\dagger}) \tag{3.28}$$

Thus, the prescription for unitarizing an approximate S-matrix employed in this study is to use Eq. (3.27b) to construct the corresponding approximate R-matrix and then "Hermitizing" this approximate R-matrix via Eq. (3.28). When $\underset{\sim}{R}_H$ is then put back into Eq. (3.27a) in place of $\underset{\sim}{R}$, a unitary S-matrix results. It is easy to show that the unitarized S-matrix, $\underset{\sim}{S}_U$, is given in terms of the approximate S-matrix by

$$\underset{\sim}{S}_U = [\underset{\sim}{S} \cdot (\underset{\sim}{1} + \underset{\sim}{S})^{-1} + \tilde{\underset{\sim}{S}} \cdot (\underset{\sim}{1} + \tilde{\underset{\sim}{S}})^{-1}] \cdot [(\underset{\sim}{1} + \underset{\sim}{S})^{-1} + (\underset{\sim}{1} + \tilde{\underset{\sim}{S}})^{-1}]^{-1} \tag{3.29}$$

where

$$\underset{\sim}{\tilde{S}} = (\underset{\sim}{S}^{+})^{-1}$$

This prescription for unitarizing an approximate S-matrix is, as mentioned, not a unique prescription. However, if the S-matrix resulting from a particular unitarization scheme is very sensitive to the scheme used, then the original S-matrix is probably far from unitary, which would cast doubt concerning the dynamical approximations employed.

Finally, the matrix of the tunneling probabilities, $\underset{\sim}{P}$, can also be obtained within the SCP-IOS approximation. A simplified form for the matrix elements will be a reasonable approximation, however, if the coupling elements $B_{k,k'}$ are small in the tunneling region. Neglecting the effect of these coupling elements results in an SCP-IOS approximation which is equivalent to the vibrationally adiabatic approximation. The matrix $\underset{\sim}{P}$ is diagonal and of the form

$$P_{\underset{\sim}{n},\underset{\sim}{n}'} = \delta_{\underset{\sim}{n},\underset{\sim}{n}'} \, e^{-2\theta} \qquad (3.30)$$

where θ is the vibrationally adiabatic barrier penetration integral

$$\theta \equiv \theta(E,\underset{\sim}{n}) = \int_{s_2}^{s_3} ds \sqrt{2(V_a(s) - E)} \qquad (3.31)$$

Eq. (3.30) is valid only for small tunneling probabilities, the more generally valid expression[46] being

$$P_{\underset{\sim}{n},\underset{\sim}{n}'} = \delta_{\underset{\sim}{n},\underset{\sim}{n}'} \left(1 + e^{2\theta}\right)^{-1} \qquad (3.32)$$

Use of the expression Eq. (3.32) can be extended so as to include energies above the top of the barrier, or for situations where there is no actual barrier to dissociation, as discussed in section III.B for the case of a Morse oscillator reaction coordinate potential. Using the turning points in Eqs. (3.17) and (3.18), the barrier penetration integral $\theta(E,\underset{\sim}{n})$ can be analytically continued[33] and is of the form of Eq. (3.18d).

D. Calculations for Model Unimolecular Systems

As a test of the model developed in sections III.A,B,C , one of the simple two oscillator models of section II was chosen for investigation. The particular example chosen is the one-barrier Henon-Heiles potential, the quantum mechanical results for which are discussed in section II.C. The potential function for this simple oscillator system is (in Cartesian coordinates)

$$V(x,y) = \frac{1}{2}\left(x^2 + y^2\right) - \frac{1}{3}x^3 - \frac{1}{3}x\,y^2 \qquad (3.33)$$

In order to apply the branching model to this system, it is first necessary to cast the potential into the form of the reaction

path Hamiltonian,[47] Eq. (3.19). For this example, the reaction path is straight (the x-axis) and the reaction path Hamiltonian thus takes the relatively simple form

$$H(p_s, s, n, q) = \frac{1}{2}\left[p_s + \frac{\omega'(s)}{2\omega(s)}(n + \frac{1}{2}) \sin 2q \right]^2 + V_o(s) + (n + \frac{1}{2})\,\omega(s) \qquad (3.34)$$

where

$$V_o(s) = s^2/2 - s^3/3 \qquad (3.35a)$$

$$\omega(s) = 1 - 2s/3 \qquad (3.35b)$$

Since the complete potential in Eq. (3.33) is already quadratic in the transverse degree of freedom (i.e., the y direction), the reaction path Hamiltonian is actually the exact Hamiltonian for this example.

The interior S-matrix, $\underset{\sim}{S}_o$, and the tunneling probability matrix $\underset{\sim}{P}$ were constructed as outlined in section III.C. The vibrationally adiabatic approximation was made for the tunneling matrix, which was therefore diagonal. By finding the various roots of the secular determinant equation, Eq. (3.7), the various metastable state eigenvalues were found. These eigenvalues, in an approximate way, correspond to the eigenvalues obtained from the exact quantum mechanical methods employed in section II.C. Figs. 20 and 17 show the results given by the present model, and the

rigorous quantum mechanical values, respectively. As discussed before, this system shows quite pronounced mode specificity in its decay rates. More important for this study, however, is the fact that the multi-channel branching model reproduces the correct results quite well, for all energies of interest. In Fig. 20, the states corresponding to energies above the barrier were obtained by utilizing the methods outlined in section III.A and by Eqs. (3.31) and (3.32). Even for these "over the barrier" states, the agreement with the exact quantum results is excellent.

E. Other Applications of the Branching Model

1. Energy Levels in a Multi-dimensional Double-well Potential

The overall S-matrix given by Eq. (3.5) is specific to the type of scattering situation depicted in Fig. 18. It is possible, of course, to apply the ideas of the branching model to situations other than that one, and thus be able to describe other types of dynamical phenomena. The object of this section is to demonstrate how the ideas of the branching model can be used to describe the energy levels of a multi-dimensional double-well potential.

Consider first inelastic scattering on a potential surface for which the potential along the reaction coordinate is as depicted in Fig. 21. The analysis of section III.A can be generalized to treat the present case (which possesses two interior wells, separated by a barrier) or any other more complicated sequence of wells and barriers.

Consider the entire region of well a , barrier 1, and well b as the "inside" region that is separated from the "outside" region by barrier 2 (see Fig. 21). If S_o is the S-matrix which characterizes this complete "inside" region (wells a and b and barrier 1), then Eq. (3.5) applies as before to give the S-matrix as

$$\underset{\sim}{S}(E) = \underset{\sim}{S}_{out} \cdot \left(\underset{\sim}{1} - \underset{\sim}{P}_2 \right)^{1/2} \cdot \underset{\sim}{S}_{in} + \underset{\sim}{S}_{out} \cdot \underset{\sim}{P}_2^{1/2} \cdot \underset{\sim}{S}_o \cdot \left[\underset{\sim}{1} + \left(\underset{\sim}{1} + \underset{\sim}{P}_2 \right)^{1/2} \cdot S_o \right]^{-1} \cdot \underset{\sim}{P}_2^{1/2} \underset{\sim}{S}_{in} \tag{3.36}$$

where $\underset{\sim}{S}_{in}$ and $\underset{\sim}{S}_{out}$ are the incoming and outgoing S-matrices for the "outside" region in Fig. 21 and $\underset{\sim}{P}_2$ the matrix of tunneling probabilities for barrier 2 . To determine the S-matrix $\underset{\sim}{S}_o$ in Eq. (3.36), i.e., the S-matrix for walls a and b, separated by barrier 1, one recognizes that this complex "inside" region is equivalent to the scattering system in Fig. 18 if one identifies the external scattering region of Fig. 18 with the region of well b in Fig. 21 . Thus, $\underset{\sim}{S}_o$ in Eq. (3.36) is itself given by Eq. (3.5) ,

$$\underset{\sim}{S}_o = \underset{\sim}{S}_{b,out} \cdot \left(\underset{\sim}{1} - \underset{\sim}{P}_1 \right)^{1/2} \cdot \underset{\sim}{S}_{b,in} + \underset{\sim}{S}_{b,out} \cdot \underset{\sim}{P}_1^{1/2} \cdot \underset{\sim}{S}_a \left[\underset{\sim}{1} + \left(\underset{\sim}{1} - \underset{\sim}{P}_1 \right)^{1/2} \cdot \underset{\sim}{S}_a \right]^{-1} \cdot \underset{\sim}{P}_1^{1/2} \cdot \underset{\sim}{S}_{b,in} \tag{3.37}$$

where $\underset{\sim}{S}_a$ is the S-matrix for motion back and forth across well a ($s_1 \to s_2 \to s_1$), $\underset{\sim}{S}_{b,in}$ is the S-matrix for inward motion across well b ($s_4 \to s_3$), $\underset{\sim}{S}_{b,out}$ the S-matrix for outward motion across well b ($s_3 \to s_4$), and $\underset{\sim}{P}_1$ the matrix of tunneling probabilities for barrier 1. The final expression for the S-matrix for the system of Fig. 21 is obtained by inserting Eq. (3.37) for $\underset{\sim}{S}_o$ into Eq. (3.36). It is straightforward to extend this procedure inductively to generate the S-matrix for the case of arbitrary number of wells and barriers.

The S-matrix given by Eq. (3.36) is the general one for the scattering situation of Fig. 21. If one is interested in bound state energy levels, however, it is necessary to modify the potential profile of Fig. 21 in the obvious way. Equivalent to making this modification is to "switch off" the tunneling through barrier 2 by setting $\underset{\sim}{P}_2 = 0$, and look for the poles of the S-matrix $\underset{\sim}{S}(E)$. With this modification, Eq. (3.36) shows that the poles occur at values of E for which

$$\det \left| \underset{\sim}{1} + \underset{\sim}{S}_o(E) \right| = 0 \qquad (3.38)$$

with $\underset{\sim}{S}_o$ given by Eq. (3.37). Appendix , of reference 56 demonstrates how expressions of this form correspond to the bound state eigenvalues calculated from quantum mechanical perturbation theory. (It is easy to show that for $\underset{\sim}{S}_o$ unitary, the roots of the Eq. (3.38) will be real, thereby corresponding to true bound state

eigenvalues.)

Inserting the expression for $\underset{\sim}{S}_o$ given by Eq. (3.37) into Eq. (3.38), yields the following determinantel equation:

$$\det \Big| \underset{\sim}{1} + \underset{\sim}{S}_{b,out} \cdot \left(\underset{\sim}{1} - \underset{\sim}{P}_1 \right)^{1/2} \cdot \underset{\sim}{S}_{b,in} + \underset{\sim}{S}_{b,out} \cdot \underset{\sim}{P}_1^{1/2} \cdot \underset{\sim}{S}_a \left[\underset{\sim}{1} + \left(\underset{\sim}{1} - \underset{\sim}{P}_1 \right)^{1/2} \cdot \underset{\sim}{S}_a \right]^{-1} \cdot \underset{\sim}{P}_1^{1/2} \cdot \underset{\sim}{S}_{b,in} \Big| = 0 \tag{3.39}$$

This can be put into a more useful form by multiplying it from the left by $\det \left| \underset{\sim}{S}_{b,in} \right|$ and from the right by $\det \left| \underset{\sim}{S}_{b,out} \right|$.

This results in the expression

$$\det \Big| \underset{\sim}{S}_b + \underset{\sim}{S}_b \cdot \left(\underset{\sim}{1} - \underset{\sim}{P}_1 \right)^{1/2} \cdot \underset{\sim}{S}_b + \underset{\sim}{S}_b \cdot \underset{\sim}{P}_1^{1/2} \cdot \underset{\sim}{S}_a \cdot \left[\underset{\sim}{1} + \left(\underset{\sim}{1} - \underset{\sim}{P}_1 \right)^{1/2} \cdot \underset{\sim}{S}_a \right]^{-1} \cdot \underset{\sim}{P}_1^{1/2} \cdot \underset{\sim}{S}_b \Big| = 0 \tag{3.40}$$

for determining the bound state eigenvalues. In Eq. (3.40), $\underset{\sim}{S}_b$, the S-matrix per oscillation in well b ($s_3 \to s_4 \to s_3$) is given by

$$\underset{\sim}{S}_b = \underset{\sim}{S}_{b,in} \cdot \underset{\sim}{S}_{b,out} \tag{3.41}$$

Note that the indices of $\underset{\sim}{S}_a$ refer to transverse vibrational states at s_2 and those of $\underset{\sim}{S}_b$ to transverse vibrational states at s_3,

and since $\underset{\sim}{P}_1$ is assumed to be vibrationally adiabatic, all the matrices in Eq. (3.40) are thus square matrices of the same dimension. Finally, by simple matrix manipulation, it is easy to cast Eq. (3.40) into the following more symmetric form

$$\det \Big| \Big[\underset{\sim}{S}_b^{-1} + \big(\underset{\sim}{1} - \underset{\sim}{P}_1 \big)^{1/2} \Big] \cdot \underset{\sim}{P}_1^{-1/2} \Big[\underset{\sim}{S}_a^{-1} + \big(\underset{\sim}{1} - \underset{\sim}{P}_1 \big)^{1/2} \Big] + \underset{\sim}{P}_1^{1/2} \Big| = 0 \qquad (3.42)$$

which demonstrates that wells a and b enter the eigenvalue equation on equal footings, as expected.

Recent quantum mechanical calculations of Bowman, et al [57], of the splittings in a symmetric double well potential, coupled to one transverse vibrational mode, provide an interesting example with which to test the branching model results of Eq. (3.42). Again, the SCP-IOS approximation of section III.C was used to construct $\underset{\sim}{S}_a$ (which is equivalent to $\underset{\sim}{S}_b$ for this example) and $\underset{\sim}{P}$. Table II shows results obtained from Eq. (3.42) for the splittings of the nearly degenerate doublets, the most sensitive quantity for such systems, compared to Bowman's quantum mechanical results. (Splittings for higher energy levels were not attempted since in this case Bowman's model potential has more than two wells.) Again, the multichannel branching model appears to provide a good description of the phenomenon.

2. Reaction Probabilities in Complex Formation

As a final application of the multi-channel branching model, consider the phenomenon of complex formation in molecular collisions. Such a system is characterized by the potential energy surface for which the potential along the reaction coordinate is sketched in Fig. 22. Reaction corresponds to motion from region a ($s \to -\infty$) to region b ($s \to +\infty$), and as before, the (F-1) transverse vibrational modes are not indicated in the figure.

To proceed, it is convenient to define $\underset{\sim}{S}_a$, $\underset{\sim}{S}_o$, and $\underset{\sim}{S}_b$ as transition amplitude matrices for the intervals $(-\infty, s_1)$, (s_2, s_3), and $(s_4, +\infty)$, respectively. These matrices are to be considered as transition amplitudes for a single pass across the well, not as a complete oscillation in it, as in section II.B. Another feature of these matrices is that they are in general rectangular since the number of transverse vibrational states that are energetically open at $s = -\infty$, s_1, s_2, s_3, s_4, and $+\infty$ are in general different. $\underset{\sim}{P}_1$ and $\underset{\sim}{P}_2$ are the tunneling probability matrices for motion across barriers 1 and 2, which can be considered to be diagonal square matrices (via the vibrationally adiabatic approximation) as described in section III.C.

The branching analysis for constructing the net scattering matrix, $\underset{\sim}{S}_{net}$, is similar to that presented in section III.A. The first trajectory (i.e., amplitude branch) which contributes to the $a \to b$ reaction process for the system in Fig. 22 corresponds to going straight across the inside well, with amplitude

$$\underset{\sim}{S}_b \cdot \underset{\sim}{P}_2^{1/2} \cdot \underset{\sim}{S}_o \cdot \underset{\sim}{P}_1^{1/2} \cdot \underset{\sim}{S}_a \qquad (3.43)$$

The next trajectory corresponds to making one extra oscillation back and forth across the inside well, with amplitude

$$- \underset{\sim}{S}_b \cdot \underset{\sim}{P}_2^{1/2} \cdot \underset{\sim}{S}_o \cdot (\underset{\sim}{1} - \underset{\sim}{P}_1)^{1/2} \cdot \underset{\sim}{S}_o^{tr} \cdot (\underset{\sim}{1} - \underset{\sim}{P}_2)^{1/2} \cdot \underset{\sim}{S}_o \cdot \underset{\sim}{P}_1^{1/2} \cdot \underset{\sim}{S}_a \qquad (3.44)$$

Note that the matrix $\underset{\sim}{S}_o^{tr}$, the transpose of $\underset{\sim}{S}_o$, is the amplitude for going across the inside well in the negative direction. By including all of the amplitude trajectories which contribute to the reactive process $a \rightarrow b$, the net amplitude (or matrix) for the reaction is

$$\underset{\sim}{S}_{b \leftarrow a}(E) = \underset{\sim}{S}_b \cdot \underset{\sim}{P}_2^{1/2} \cdot \underset{\sim}{S}_o \cdot [\underset{\sim}{1} + (\underset{\sim}{1} - \underset{\sim}{P}_2)^{1/2} \cdot \underset{\sim}{S}_o^{tr} \cdot (\underset{\sim}{1} - \underset{\sim}{P}_2)^{1/2} \cdot \underset{\sim}{S}_o]^{-1} \cdot \underset{\sim}{P}_1^{1/2} \cdot \underset{\sim}{S}_a \qquad (3.45)$$

By calculating the matrices in Eq. (3.45) by some dynamical approximations such as those described in section III.C, one would have an approximate state-to-state reactive transition amplitude, along with other dynamical information. For example, the energy dependence of the net matrix $\underset{\sim}{S}_{net}(E)$ will in general show the complicated resonance structure corresponding to the formation and decay of metastable states (i.e., collision complexes) in the inside well region. The energies and lifetimes of these individual metastable states are given, as in section III.B, by the poles of the S-matrix[13], which from Eq. (3.45) are the complex energies E for

which the following determinantal equation is satisfied:

$$\det \left| \underset{\sim}{1} + \left(\underset{\sim}{1} - \underset{\sim}{P}_1 \right)^{1/2} \cdot \underset{\sim}{S}_o^{tr} \cdot \left(\underset{\sim}{1} - \underset{\sim}{P}_2 \right)^{1/2} \cdot \underset{\sim}{S}_o \right| = 0 \tag{3.46}$$

For many applications, however, one is interested in a somewhat less detailed level of experimental measurable, e.g., in an energy averaged reaction probability. This is equivalent to neglecting all the cross terms in constructing the reaction probabilities

$$\left(\underset{\sim}{P}_{b,a} \right)_{n,n'} = \left| \left(\underset{\sim}{S}_{o,a} \right)_{n,n'} \right|^2 \tag{3.47}$$

The branching model (now a classical probability branching model[49]) for this average reaction probability thus becomes

$$\begin{aligned} \underset{\sim}{P}_{b \leftarrow a} = & \underset{\sim}{P}_b \cdot \underset{\sim}{P}_2 \cdot \underset{\sim}{P}_o \cdot \underset{\sim}{P}_1 \cdot \underset{\sim}{P}_a \\ & + \underset{\sim}{P}_b \cdot \underset{\sim}{P}_2 \cdot \underset{\sim}{P}_o \cdot \left(\underset{\sim}{1} - \underset{\sim}{P}_1 \right) \cdot \underset{\sim}{P}_o^{tr} \cdot \left(\underset{\sim}{1} - \underset{\sim}{P}_2 \right) \cdot \underset{\sim}{P}_o \cdot \underset{\sim}{P}_1 \cdot \underset{\sim}{P}_a \\ & + \ldots \end{aligned} \tag{3.48}$$

where the rectangular matrices $\underset{\sim}{P}_a$, $\underset{\sim}{P}_o$, and $\underset{\sim}{P}_b$ are defined by

$$\left(\underset{\sim}{P}_a \right)_{n,n'} = \left| \left(\underset{\sim}{S}_a \right)_{n,n'} \right|^2 \tag{3.49}$$

etc. Eq. (3.48) is a geometric matrix series that is easily summed to give

$$\underset{\sim}{P}_{b\leftarrow a} = \underset{\sim}{P}_{b} \cdot \underset{\sim}{P}_{2} \cdot \underset{\sim}{P}_{o} \cdot \left[\underset{\sim}{1} - (\underset{\sim}{1} - \underset{\sim}{P}_{1}) \cdot \underset{\sim}{P}_{o}^{tr} \cdot (\underset{\sim}{1} - \underset{\sim}{P}_{2}) \cdot \underset{\sim}{P}_{o} \right]^{-1} \cdot \underset{\sim}{P}_{1} \cdot \underset{\sim}{P}_{a} \qquad (3.50)$$

Such a result as Eq. (3.50) has no resonance structure in its energy dependence, for this detail of information is lost when the interference between the different trajectories that contribute to the $a \rightarrow b$ reaction is neglected.

The analysis in Eqs. (3.48) - (3.50) is actually a multi-channel version of a result which has been given previously, known as the unified statistical model.[58] In fact, in the limit of one dimension, the result of Eq. (3.50) can be shown to be equivalent to the results of the unified statistical model. Therefore, the multi-channel branching model has provided a way of extending the results to include the effects of vibrational inelasticity as one moves along the reaction coordinate, which is certainly a more realistic model when dealing with real polyatomic collision systems.

IV. Mode Specificity in Formaldehyde Decomposition

Results of exact quantum mechanical calculations of metastable state decay constants for model systems (see sections I, II) have demonstrated two types of mode specificity. First, some systems manifested a dynamical mode specificity, by which is meant that the intramolecular couplings are such that energy redistribution among the vibrational modes of the molecule is very slow (though not strictly zero) compared to reaction rates. If there are certain symmetries in the Hamiltonian for the system, a second type of mode specificity can exist, i.e., a symmetry-induced mode specificity. Here if the molecular system possesses a definite symmetry throughout the entire course of reaction , it is possible to find decaying states belonging to different irreducible representations which therefore cannot transfer energy to each other (a sort of intramolecular dynamical selection rule). This second type of mode specificity has recently been discussed[59] in detail in the context of transition state theory, including application to the formaldehyde unimolecular decomposition reaction.

To this point, such detailed dynamical studies as these have been restricted to model systems possessing only two degrees of freedom. Section III proposes a method which can, in principle, be applied to more realistic polyatomic unimolecular systems with semi-quantitative accuracy. Though such an approach may prove to be inevitably necessary, it still retains much of the computational intractability

associated with the exact quantum approaches. An alternate approach would be to somehow reduce the dimensionality of the system being investigated so as to retain the essential dynamical information being sought. Such approximations with application to scattering systems have recently been reported.[60]

The unimolecular decomposition of formaldehyde represents a particularly interesting example of a polyatomic system to be investigated. Though it has received extraordinary attention over the past several years, both experimentally and theoretically,[61] there remain many unresolved questions as to the details of the overall photochemical mechanism,[62] grossly depicted in Eq. (4.1):

$$H_2CO + h\nu \rightarrow H_2CO^{*}\ (S_1) \qquad (4.1a)$$

$$H_2CO^{*}\ (S_1) \rightarrow H_2CO^{\ddagger}\ (S_o) \qquad (4.1b)$$

$$H_2CO^{\ddagger}\ (S_o) \rightarrow H_2 + CO \qquad (4.1c)$$

The interest of this study, of course, focuses on the last two steps of the above mechanism, especially on the unimolecular decomposition step (Eq. (4.1c)) which occurs on the ground electronic (S_o) surface.

The radiationless transition from the S_1 electronic surface to the S_o surface "prepares" the formaldehyde system in some high energy ro-vibrational state which can then dynamically evolve to eventually yield molecular products, H_2 and CO. The question to be addressed is how the individual metastable states (correspond-

ing to different initial distributions of energy among the modes of the molecule) behave in their decay rate constants, i.e., whether they exhibit mode-specificity, be it dynamical or symmetry-induced.

The unique role of the out-of-plane bending mode has also been the subject of some interest[63] in regard to formaldehyde photochemistry. The S_1 electronic state geometry, being non-planar, gives rise (in the Franck-Condon sense) to significant population in the planar ground electronic state's out-of-plane bending mode initially. Since this is the only out-of-plane motion among the ground state vibrations, it is clear from symmetry considerations alone that energy cannot be directly transferred into or out of this mode from the other modes of the molecule (at least for small amplitude vibrations), with the exception of the mode corresponding to the reaction coordinate (which obviously cannot be harmonic). A pertinent question, therefore, revolves around how the out-of-plane bend couples to the reaction coordinate motion, and whether just considering these two degrees of freedom should yield relevant information about the mode-specificity of the full-dimensional system. In other words, are the indirect couplings between the other modes and the out-of-plane mode (via the reaction coordinate) negligible so as to allow them to be separated out of the problem? Such a separation would, of course, allow a more rigorous treatment of the dynamics, i.e., a quantum mechanical treatment as described in sections I and II .

Such dynamical studies as these require the determination of the potential energy surface for all relevant configurations of the nuclei in the ground electronic surface, S_o . To this end, the reaction path Hamiltonian method of Miller, Handy, and Adams[47] (see also section III.C) was employed to construct the Hamiltonian for the decomposition process

$$H_2CO \quad (S_o) \quad \rightarrow \quad H_2 \; + \; CO \qquad (4.2)$$

The basic idea, as previously discussed, is to follow the gradient path (in mass weighted Cartesian coordinates) on the electronic surface from the saddle-point (or transition state) to both reactants and products. At each point along the gradient (or reaction) path, a projected force constant matrix is diagonalized, yielding normal mode frequencies for the vibrations orthogonal to the reaction path. These frequencies, of course, are dependent on the position along the reaction coordinate, and along with their corresponding eigenvectors give rise to the couplings between the various modes as one goes from reactants to products.

Once the Hamiltonian for the process has been obtained, it is possible to perform various types of dynamical calculations using various levels of theory, e.g., classical or quantum mechanical. The aim of this study of formaldehyde decomposition is to investigate the mode specificity of the individual decay rate constants, and therefore the more rigorous quantum mechanical approaches are required.

Sections IV.A, B will describe the Hamiltonian used for this system, as well as the justification for neglecting all the vibrational modes except the out-of-plane bend and the reaction coordinate mode in ascertaining the mode specific character of the decay rates.

A. The Hamiltonian

The potential energy surface for the S_0 electronic state of formaldehyde leading from reactant to molecular products has been characterized previously at various levels of approximation.[64] Calculation of electronic energies at enough points on a grid the six degrees of freedom for formaldehyde by ab initio techniques to yield a surface amenable to dynamics calculations is formidable. However, by employing the methodology of the reaction path Hamiltonian of Miller, Handy, and Adams,[47] one can generate the surface for all geometries surrounding the relevant reaction path with much less computational effort. The general form for the reaction path Hamiltonian is given in section III.C, and is reproduced below for the specific example of formaldehyde (i.e., six vibrational degrees of freedom, neglecting overall rotation):

$$H(p_s,s,\underset{\sim}{n},\underset{\sim}{q}) = \frac{1}{2}\Big[\, p_s - \sum_{k,k'=1}^{5} B_{k,k'}(s)\sqrt{(2n_k+1)(2n_{k'}+1)}\times\sqrt{\omega_{k'}/\omega_k}\,\sin q_k \cos q_{k'}\,\Big]^2$$

$$\times\Big[\,1+\sum_{k=1}^{5} B_{k,6}(s)\sqrt{(2n_k+1)/\omega_k(s)}\,\sin q_k\,\Big]^{-2}$$

$$+ V_o(s) + \sum_{k=1}^{5} (n_k + \frac{1}{2}) \omega_k(s) \qquad (4.3)$$

Here s represents the reaction coordinate (or position along the gradient in mass-weighted Cartesian coordinates), p_s is its conjugate momentum, $(\underset{\sim}{n}, \underset{\sim}{q})$ are the action angle variables[54] for vibrational modes transverse to the reaction coordinate, $\omega_k(s)$ are the s-dependent frequencies of these transverse vibrational modes, and $B_{k,k'}(s)$ is a matrix of coupling functions defined in detail in reference 47.

For this calculation, the transition state geometry calculated by Schaefer, et al[64], was used. All evaluations of electronic energies, energy gradients, and second derivatives were done at the SCF level (self-consistent field), with double zeta plus polarization basis sets. The vibrational frequencies at the transition state and at the equilibrium formaldehyde geometry as well as the barrier height at the transition state, are given in Table [illegible] along with the best estimates for these quantities from higher levels of theory or from experiment.[64] The calculated function $\omega_1(s)$ corresponding to the out-of-plane bend is shown in Fig. [illegible], and the potential energy profile $V_o(s)$ is shown in Fig. [illegible]. The other frequency functions as well as the coupling functions $B_{k,k'}(s)$ are not presented here since they do not enter directly into any of the calculations to be presented later. Note that the $\omega_1(s)$ for the out-of-plane bend has been scaled [illegible]

from higher level of theory, and the function $V_o(s)$ has been adjusted to give the best barrier height estimates as well as the imaginary frequency of the transition state. Similar results have been reported previously by Fukui, et al,[65] for the formaldehyde system, but no coupling functions are included in their work. The smooth curves shown in Figs. 23 and 24 were obtained by fitting the discrete geometry points with one-dimensional spline functions.*

The Hamiltonian of Eq. (4.3) (including the fits for the functions $\underset{\sim}{\omega}(s)$, $\underset{\sim}{b}(s)$, and $V_o(s)$) could, in principle, be used directly in dynamical calculations, such as classical trajectory or semi-classical studies. Even if the dimensionality of the system were tractable, however, the Hamiltonian (Eq. (4.3)) would need to be transformed if quantum mechanical calculations were to be carried out.[66]

A principle feature of the results for this system is that the reaction coordinate (and hence the functions $\omega(s)$ and $V_o(s)$) is symmetric about the equilibrium geometry ($s = 0$). This is most easily visualized by noting that there are two equivalent transition states obtained by reflecting through the principle axis of the molecule.[64] Thus, there are two equivalent barriers to reaction for this dissociation process.

---

* Note: The calculation of the reaction path Hamiltonian described above was carried out by Dr. S. K. Gray (Ph. D. thesis, Department of Chemistry, University of California, Berkeley, Berkeley, Calif.)

B. Dynamical Results

Quantum mechanical calculations on the full six-dimensional Hamiltonian (with total J = 0) of section IV.A are, at present, not computationally feasible. However, careful consideration of the coupling functions $\underset{\sim}{B}(s)$ reveals that a reduction in the number of degrees of freedom (from six to two) is a reasonable approximation.

The out-of-plane bend (shown in Fig. 23) has strictly zero direct coupling to all other transverse modes, i.e., $B_{5,k} = 0$ for all $k \neq 5$. Thus, in any dynamical calculation, energy could never be transferred directly from the out-of-plane bend to the other modes of the molecule, except to the reaction coordinate mode. Further, the direct coupling to the reaction coordinate occurs not through the function $B_{5,6}(s)$ (which is also zero), but through variation of the frequency $\omega(s)$ as one moves along the reaction path (see Fig. 23). Of course, all modes couple indirectly (via the reaction coordinate) to the out-of-plane bend, but if such indirect couplings are weak, it should be reasonable to neglect the other modes entirely and still retain the pertinent features of the dynamics, i.e., the mode specific character of the system should still be exhibited as it would be for the entire full-dimensional system.

The Hamiltonian used for the two degrees of freedom is thus of the form

$$H(p_s,s,n,q) = \frac{p_s^2}{2} + V_o(s) + (n + \tfrac{1}{2})\,\omega(s) \qquad (4\ 4)$$

where it is also assumed that the term $\omega'(s)/\omega(s)$ in the kinetic energy expression of Eq. (4.3) is negligible.

For purposes of computation, the functions $\omega(s)$ and $V_o(s)$ were fit (by non-linear least squares fitting procedures) to polynomials in s^2 (recall the symmetry of the Hamiltonian about s = 0), of the following forms:

$$V_o(s) = a_2 s^2 + a_4 s^4 \tag{4.5a}$$

$$\omega(s) = b_o + b_2 s^2 + b_4 s^4 + b_6 s^6 + b_8 s^8 + b_{10} s^{10} \tag{4.5b}$$

Values for the coefficients in Eqs. (4.5) are given in Table IV, and the functions are depicted in Figs. 23 and 24 for comparison to the ab initio functions. The purpose of re-fitting the functions in powers of s^2 is to allow for analytical evaluation of the quantum mechanical matrix elements necessary for application of the complex scaling method.

In addition, calculations were most easily carried out in Cartesian (mass-weighted) coordinates, the Hamiltonian being given by

$$H(p_s,s,p_x,x) = \frac{p_s^2}{2} + V_o(s) + \frac{p_x^2}{2} + \frac{\omega^2(s)}{2} x^2 \tag{4.6}$$

with (p_s, s) as before, and (x, p_x) being the out-of-plane position and conjugate momentum, respectively.

Calculations of the metastable state decay rates for this simplified two dimensional system were performed by the complex scaling method,[17] described in detail in section I.C. The scaled Hamiltonian for this system has the following form

$$H_\alpha = -\frac{\hbar^2}{2} e^{-2i\alpha} \frac{\partial^2}{\partial s^2} + V_o(se^{i\alpha}) - \frac{\hbar^2}{2} \frac{\partial^2}{\partial x^2}$$

$$+ \frac{\omega^2(se^{i\alpha})}{2} x^2 \qquad (4.7)$$

The basis set used for expanding the Hamiltonian of Eq. (4.7) was related to the simple harmonic oscillator basis set for each degree of freedom. Results of the calculation for the formaldehyde system are shown in Fig. 25. Only states above 70 kcal/mole total energy were obtainable due to precision limitations as well as basis set size limitations. However, the states obtained in this energy region (near the classical threshold) are the relevant ones experimentally.[28,29]

The Hamiltonian (Eq. (4.6)) possesses C_{2v} symmetry, the states corresponding to it therefore falling into one of four irreducible representations: A_1, A_2, B_1, and B_2. In addition, the Hamiltonian possessed a reflective symmetry with respect to the reaction coordinate at every point in space, therefore giving rise to an evenness and oddness in the out-of-plane bend vibrational states which is preserved all along the reaction coordinate. As

discussed in detail elsewhere,[59] this gives rise to a symmetry-induced mode specificity, which can easily be seen by inspection of Fig. 25. Out-of-plane bending states only couple with other out-of-plane bending states with the same evenness or oddness, even-odd coupling being strictly zero because of the symmetry of the Hamiltonian about the reaction path (i.e., the line $x = 0$). Metastable states with "even" out-of-plane contributions have faster decay rates because they lead to a build-up of probability density at the critical barrier region. Metastable states with "odd" out-of-plane contributions have slower decay rates because of the relative lack of probability density at the barrier regions. Even if the formaldehyde system exhibited only statistical behavior (i.e., if there was no dynamical mode specificity), this symmetry-induced mode specificity would still cause states with different irreducible representations to decay with different rates.[59]

Fig. 25, however, demonstrates that for this formaldehyde decomposition system, even the dynamical mode specificity is significant, there being several states (within the same irreducible representation) with almost the same energies having significantly different decay rates (differing by up to two orders of magnitude for the states shown).

It should be noted that the reported calculations include from 0 to 7 quanta in the out-of-plane bending mode, and therefore fall well within the range of experimental interest.[28]

Classical trajectory studies[25] for the system whose Hamiltonian is given by Eq. (4.6) reveal that there does exist a transition in character from quasi-periodic to chaotic as one goes from low to higher energies. It is interesting to note that this system displays a significant degree of dynamical mode specificity in its decay rates, yet classically exhibits chaotic intramolecular dynamics. All of the states shown in Fig. 25 lie well within this classical ergodic region.

C. Effects of Other Modes

The significance of the results presented in section IV.B depend directly on the validity of the approximation of reducing the problem from the full dimensionality of the formaldehyde surface. By including a third mode (e.g., an HCH rocking mode), this approximation can be tested. The Hamiltonian used has the form

$$H = \frac{p_s^2}{2} + V_o(s) + \frac{p_x^2}{2} + \frac{\omega_x^2(s)}{2} x^2 + \frac{p_y^2}{2} + \frac{\omega_y^2(s)}{2} y^2 + A y (s^2 - B s^4) \qquad (4.8)$$

where the new mode (with coordinate y and momentum p_y) has been included. By inspection, there is no direct coupling between modes x and y, but the third mode can couple indirectly (via the reaction coordinate, s) to the out-of-plane bending mode. Also, note that the third mode contributes to the curvature of the reaction path

through the term

$$A\,y\,(s^2 - B\,s^4) \tag{4.9}$$

At least qualitatively, this is representative of the type of coupling present in the full-dimensional formaldehyde Hamiltonian of section IV.A.

So as to be able to perform the exact quantum mechanical calculations for this three degree of freedom system, the effective value of $\hbar$ in Eq. (4.8) had to be increased so as to include fewer states in the metastable well (per degree of freedom). Results are shown in Figs. 26, 27, and 28. Fig. 26 shows results holding the frequency ω_y constant (i.e., no coupling to the y-mode), Fig. 27 has the frequency ω_x constant (i.e., no coupling to the x-mode), and Fig. 30 shows the full system of Eq. (4.8) where modes x and y can couple indirectly via the reaction coordinate.

The main result is that there appears to be no noticeable effect on the mode specific character of the two mode system of section IV.B by inclusion of the third, indirectly coupled, mode. This therefore appears to indicate that the degree of mode specificity (both dynamical and symmetry-induced) exhibited in Fig. 25 will carry over for the full-dimensional Hamiltonian (Eq. (4.3)) for formaldehyde decomposition.

D. Discussion

It is interesting to compare the exact dynamical results of section IV.B with results obtained based upon statistical theories

of unimolecular reaction rates, i.e., the RRKM theory. Even by taking into account the effects of symmetry in the statistical treatment (see reference 59 for an example), it is seen that the dynamical results are much more complex (due to dynamical mode specificity) than previously expected. Whether or not this apparent mode specificity of the formaldehyde system can be taken advantage of or observed remains a very difficult experimental question. Preparation of the formaldehyde system on the ground electronic surface in a particular vibrational energy distribution among the modes is complicated due to the indirectness of the mechanism, Eq. (4.1), as well as non-adiabatic effects which still influence the dynamics of the system once it has reached the S_o surface. However, as pointed out by Miller,[59] such a preparation should at least lead to some preservation of the evenness or oddness of the out-of-plane bending mode states, thus enabling experimentalists to take advantage of the symmetry-induced mode specificity possessed by the system.

Of course, preparation of the high energy vibrational states directly (without recourse to a second electronic surface) would ideally serve to test the theories and results presented here. Whether or not such preparations can be achieved for the formaldehyde system is still a question of some interest,[67] not only for the formaldehyde system, but for other unimolecular systems as well.

References

1. F. A. Lindemann, Trans. Faraday Soc., 17, 598 (1922).
2. See, for example, (a) P. J. Robinson and K. A. Holbrook, Unimolecular Reactions, Wiley, New York, 1972; (b) W. Forst, Theory of Unimolecular Reactions, Academic, New York, 1973; (c) R. A. Marcus, J. Chem. Phys., 20, 359 (1952); (d) N. B. Slater, Theory of Unimolecular Reactions, Cornell University Press, Ithaca, New York, 1959.
3. See, for example, (a) K. J. Laidler, Theories of Chemical Reaction Rates, McGraw-Hill, New York, 1969; (b) H. Eyring, Trans. Faraday Soc., 34, 41 (1938).
4. See, for example, reference 2b, pp. 344-347.
5. See, for example, W. L. Hase in Dynamics of Molecular Collisions Part B, Vol. 2 of Modern Theoretical Chemistry, edited by W. H. Miller, Plenum, New York, 1976.
6. (a) F. W. Schneider and B. S. Rabinovitch, J. Amer. Chem. Soc., 84, 4215 (1962), and other references cited in reference 5; (b) I. Oref and B. S. Rabinovitch, Acc. Chem. Res., 12, 166 (1979).
7. See reference 5, p. 123.
8. See, for example, (a) Advances in Laser Chemistry, edited by A. H. Zewail, Springer, New York, 1978; (b) Laser-induced Processes in Molecules, edited by K. L. Lompa and S. D. Smith, Springer, New York, 1979.

9. R. E. Smalley, D. H. Levy, and L. Wharton, J. Chem. Phys., 64, 3266 (1976); M. S. Kim, R. E. Smalley, L. Wharton, and D. H. Levy, J. Chem. Phys., 65, 1216 (1976).

10. (a) K. V. Reddy and M. V. Berry, Chem. Phys. Lett., 66, 223 (1979); (b) R. Namaan, D. H. Lubman, and R. N. Zare, J. Chem. Phys., 71, 4192 (1979); (c) R. B. Hall and A. Kaldor, J. Chem. Phys., 70, 4027 (1979).

11. See, for example, (a) S. A. Rice, reference 8a, p. 2; (b) R. A. Marcus, D. W. Noid, and M. L. Koszykowski, reference 8a, p. 298.

12. See, for example, (a) D. L. Bunker, J. Chem. Phys., 37, 393 (1962); 40, 1946 (1964); (b) E. Thiele and D. J. Wilson, J. Chem. Phys., 35, 1256 (1961); 38, 1959 (1963).

13. See, for example, T.-Y. Wu and T. Ohmura, Quantum Theory of Scattering, Prentice Hall, Englewood Cliffs, 1962.

14. See, for example, W. H. Miller, Adv. Chem. Phys., 30, 77 (1975).

15. W. H. Miller, J. Amer. Chem. Soc., 101, 6810 (1979).

16. B. Barbanis, Astron. J., 71, 415 (1966).

17. (a) B. Simon, Ann. Math., 97, 247 (1973); (b) E. Balslev and J. M. Combes, Commun. Math. Phys., 22, 280 (1971); (c) Int. J. Quantum Chem., 14, No. 4 (1978), the entire volume dealing with the complex scaling method.

18. A. J. F. Siegert, Phys. Rev., 56, 750 (1939).

19. See, for example, J. A. Beswick and J. Jortner, J. Chem. Phys., 68, 2277 (1978); 69, 512 (1978).

20. (a) A. D. Isaacson, C. W. McCurdy, and W. H. Miller, Chem. Phys., 34, 311 (1978); (b) J. N. Bardsley and B. R. Junker, J. Phys. B,

5, L178 (1972); (c) R. A. Bain, J. N. Bardsley, B. R. Junker, and C. V. Sukumar, J. Phys. B, 7, 2189 (1974).

21. See, for example, P. M. Morse and H. Feshbach, Methods of Theoretical Physics, McGraw-Hill, New York, 1953, p. 401.

22. (a) T. N. Resigno, C. W. McCurdy, and A. E. Orel, Phys. Rev. A, 17, 1931 (1978); (b) B. R. Junker and C. L. Huang, Phys. Rev. A, 18, 313 (1978).

23. M. J. Davis and E. J. Heller, J. Chem. Phys., 71, 3383 (1979).

24. N. Moiseyev, P. R. Certain, and F. Weinhold, Int. J. Quantum Chem., 14, 727 (1978).

25. For a review, see J. Ford, Adv. Chem. Phys., 24, 155 (1973); Also, see H. Poincare, New Methods of Celestial Mechanics, Vol. 3 (1897), translated by NASA, Washington, D.C., 1967, Document N67-27279.

26. See, for example, R. N. Porter and L. M. Raff, in Dynamics of Molecular Collisions Part B, Vol. 2 of Modern Theoretical Chemistry, edited by W. H. Miller, Plenum, New York, 1976, p. 1.

27. See, for example, (a) D. L. Bunker and W. L. Hase, J. Chem. Phys., 59, 4621 (1973); (b) S. B. Woodruff and D. L. Thompson, J. Chem. Phys., 71, 376 (1979); also see (c) references cited in reference 5.

28. See: (a) E. S. Yeung and C. B. Moore, J. Chem. Phys., 58, 3988 (1973); (b) P. L. Houston and C. B. Moore, J. Chem. Phys., 65, 757 (1976), and references cited therein.

29. See reference 15, and references cited therein.

30. (a) T. F. George and W. H. Miller, J. Chem. Phys., 56, 5722 (1972); (b) 57, 2458 (1972); (c) J. D. Doll, T. F. George, and W. H. Miller, J. Chem. Phys., 58, 1343 (1973).

31. C. Cerjan, private communication.

32. (a) R. A. Marcus, J. Chem. Phys., 46, 959 (1967); (b) R. A. Marcus and M. E. Coltrin, J. Chem. Phys., 67, 2609 (1977).

33. N. Froman and P. O. Froman, JWKB Approximation, North-Holland, Amsterdam, 1965.

34. H. Goldstein, Classical Mechanics, Addison-Wesley, Reading, Mass., 1950.

35. See, for example, D. L. Bunker, Theory of Elementary Gas Reaction Rates, Pergamon, New York, 1966, p. 70.

36. See, for example, V. I. Arnold and A. Avez, Ergodic Problems of Classical Mechanics, Benjamin, New York, 1968, ch. 4.

37. See, for example, (a) Stochastic Behavior in Classical and Quantum Hamiltonian Systems, edited by J. Elhers, K. Kepp, R. Kippenhahn, H. A. Weidenmiller, and J. Zittartz, Springer, New York, 1979; (b) M. Tabor, Adv. Chem. Phys., 46, 73 (1981).

38. N. Pomphrey, J. Phys. B, 7, 1910 (1974); (b) S. Nordholm and S. A. Rice, J. Chem. Phys., 61, 203, 768 (1974); (c) R. M. Stratt, N. C. Handy, and W. H. Miller, J. Chem. Phys., 71, 3311, (1980); (d) G. Hose and H. S. Taylor, J. Chem. Phys., to be published; (e) D. W. Oxtoby and S. A. Rice, J. Chem. Phys., 65, 1676 (1976); (f) K. G. Kay, J. Chem. Phys., 61, 5205 (1974); see also (g) J. Phys. Chem. (Proceedings of 1981 American Con-

ference on Theoretical Chemistry), to be published.

39. J. Henon and C. Heiles, Astron. J., 69, 73 (1964).

40. R. J. Wolf and W. L. Hase, J. Chem. Phys., 73, 3779 (1980).

41. See, for example, C. Cohen-Tannoudji, B. Diu, and F. Laloe, Quantum Mechanics, J. Wiley, New York, 1977, p. 727.

42. See, for example, H. S. Johnston, Gas Phase Reaction Rate Theory, Ronald, New York, 1966, p. 263.

43. (a) S. K. Gray, W. H. Miller, Y. Yamaguchi, and H. F. Schaefer, J. Chem. Phys., 73, 2733 (1980); (b) S. K. Gray, W. H. Miller, Y. Yamaguchi, and H. F. Schaefer, J. Amer. Chem. Soc., 103, 1900, 1904 (1981).

44. E. J. Heller and M. J. Davis, J. Phys. Chem., 85, 307 (1981).

45. See, for example, S. Chapman, B. C. Garrett, and W. H. Miller, J. Chem. Phys., 64, 502 (1976).

46. (a) W. H. Miller, Adv. Chem. Phys., 30, 77 (1975); see also (b) W. H. Miller, J. Phys. Chem., 83, 960 (1979).

47. W. H. Miller, N. C. Handy, and J. E. Adams, J. Chem. Phys., 72, 99 (1980).

48. W. H Miller and S.-h. Shi, J. Chem. Phys., 75, 2258 (1981).

49. See, for example, J. O. Hirschfelder and E. P. Wigner, J. Chem. Phys., 7, 616 (1939), for a discussion of a probability branching model in relation to transition state theory and statistical theory. See also reference 58.

50. R. P. Feynman and A. R. Hibbs, Quantum Mechanics and Path Integrals, McGraw-Hill, New York, 1965.

51. See, for example, M. S. Child, Molecular Collision Theory, Academic Press, New York, 1974.

52. P. M. Morse, Phys. Rev., 34, 57 (1929).

53. See, for example, W. H. Miller and F. T. Smith, Phys. Rev. A, 17, 939 (1978).

54. See, for example, D. J. Kouri in Atom Molecule Collision Theory, edited by R. B. Bernstein, Plenum, New York, 1979.

55. See, for example, J. R. Taylor, Scattering Theory, Wiley, New York, 1972, p. 280.

56. B. A. Waite and W. H. Miller, J. Chem. Phys., 76, 2412 (1982).

57. K. M. Christoffel and J. M. Bowman, J. Chem. Phys., 74, 5057 (1981).

58. W. H. Miller, J. Chem. Phys., 65, 2216 (1976).

59. W. H. Miller, J. Amer. Chem. Soc., to be published.

60. S. D. Schwatz and W. H. Miller, J. Chem. Phys., to be published.

61. See, for example, (a) D. F. Heller, M. L. Elert, and W. M. Gelbart, J. Chem. Phys., 69, 4061 (1978); (b) W. M. Gelbart, M. L. Elert, and D. F. Heller, Chem. Rev., 80, 403 (1980), and references cited therein.

62. See, for example, N. J. Turro, Modern Molecular Photochemistry, Benjamin, New York, 1978.

63. C. B. Moore and J. A. Pople, private communications.

64. (a) J. D. Goddard and H. F. Schaefer, J. Chem. Phys., 70, 5117 (1979); (b) S. Carter, I. M. Mills, and J. N. Murrell, Mol. Phys., 39, 455 (1980); (c) N. C. Handy and S. Carter, Chem. Phys. Lett., 79, 118 (1981); (d) J. D. Goddard, Y. Yamaguchi, and H. F. Schaefer, J. Chem. Phys., 75, 3459 (1981).

65. Y. Yamashita, T. Yamake, and K. Fukui, Chem. Phys. Lett., 84, 123 (1981).

66. See W. H. Miller in Potential Energy Surfaces and Dynamics Calculations (ACS Symp. Series), edited by D. G. Truhlar, Plenum, New York, 1981, p. 265.

67. See, for example, (a) reference 10a; (b) B. Henry, Acc. Chem. Res., 10, 207 (1977).

Table I. Potential Parameters[a]

Figure	ω_x	ω_y	$\omega_y^{\ddagger}$[b]	η	V_2	$\hbar$	m
2	14.14	14.14	14.14	0.	0.	.5	1
3	14.14	14.14	7.27	2.0	0.	.5	1
4	14.14	14.14	14.14	0.	20.	.5	1
5	14.14	14.14	7.27	2.0	20.	.5	1
6	14.14	8.94	4.60	2.0	20.	.5	1
7	14.14	11.05	5.68	2.0	20.	.5	1
8	14.14	17.89	9.20	2.0	20.	.5	1
9	14.14	14.14	14.14	0.	170.	.4	1

[a]For the potential function of Eq. (1.13).

[b]The local frequency of the y-mode at the saddle point on the potential surface.

Table II. Energy Level Splittings in a Two-Dimensional Symmetric Double Well Potential.

	Splittings (cm^{-1})		
	Transverse Quantum No., n_y	Branching Model Results[a]	Exact Quantum Results[b]
Lowest Doublet	0	0.91	0.95
	1	1.23	1.28
	2	1.68	1.77
First Excited Doublet	0	47.2	44.4

[a] Present results (see section III.E.1)

[b] From reference 57.

Table III. Potential Parameters for Formaldehyde Decomposition to Molecular Products

Frequencies of H_2CO Equilibrium Geometry (cm^{-1})	SCF-DZ	EXP.
ω_1	3315.	3009.
ω_2	3223.	2944.
ω_3	1878.	1764.
ω_4	1585.	1563.
ω_5	1324.	1191.
ω_6	1349.	1287.
Frequency of Transition State (cm^{-1})	2320i	2124i [a]
Barrier Height (kcal/mole)	113.7	92.[b]

[a] From DZ + P CI calculation (reference 64)

[b] Best estimate (non-zero point corrected), reference 64.

Table IV. Coefficients for polynomial fits to $\omega(s)$ and $V(s)$

$\omega(s)^c = b_o + b_2 s^2 + b_4 s^4 + b_6 s^6 + b_8 s^8 + b_{10} s^{10}$ (s in $\sqrt{\text{amu}}$ Å)

$b_o = 1191.$ $b_2 = -511.755$ $b_4 = -343.317$

$b_6 = 520.867$ $b_8 = -159.227$ $b_{10} = 14.186$

$V(s)^d = a_2 s^2 + a_4 s^4$ (s in $\sqrt{\text{amu}}$ Å)

$a_2 = 93.87755$ $a_4 = -23.94835$

[c] $\omega(s)$ in cm^{-1}

[d] $V(s)$ in kcal/mole

Figure Captions

Figure 1. Profile of the potential energy $V_1(x)$ for the reaction coordinate motion; the exact functional form is given by Eq. (1.13a).

Figure 2. State-specific decay rates, $k = \Gamma/\hbar$, for the quasi-bound states of the two-oscillator system with Hamiltonian defined by Eq. (1.5), with zero coupling between the modes ($V_c = 0$).

Figure 3. Same as Figure 2, except that now coupling is included. See Table I for parameters.

Figure 4. Same as Figure 3. See Table I for parameters.

Figure 5. Same as Figure 3. See Table I for parameters.

Figure 6. Same as Figure 3. See Table I for parameters.

Figure 7. Same as Figure 3. See Table I for parameters.

Figure 8. Same as Figure 3. See Table I for parameters.

Figure 9. Same as Figure 3. See Table I for parameters. The vertical dashed lines indicate the energies of the onset of classical stochasticity and the classical threshold, respectively.

Figure 10a. A schematic representation of the cumulative tunneling probability for a single trajectory. $\{ t_k \}$ indicate the times at which the trajectory "hits" the barrier (i.e., experiences a classical turning point), and $\{ P_k \}$ are the tunneling probabilities for these "hits."

Figure 10b. A typical example of the averaged survival probability, $\langle P_s(t) \rangle_{E,n_y}$, defined by Eqs. (1.34) - (1.40). Note that the probability decays in an exponential fashion.

Figure 11. Rate constants as a function of total energy, for the same potential parameters as for Figure 7 (see Table I). The points are the quantum mechanical values, and the solid curves are the classical plus tunneling model results for the rates $k_{n_y}(E)$, obtained as outlined in section I.D.

Figure 12. Quantum mechanical rate constants versus energy for the metastable states of the Henon-Heiles potential energy surface (Eq. (2.5)), with $\hbar = 0.04$. Solid points are A_1 states, squares are A_2 states, and circles denote E states. The solid curve is the statistical (RRKM + tunneling) rate defined in Eqs. (2.11), (2.15), and (2.16).

Figure 13. Same as Figure 12, with $\hbar = 0.03$.

Figure 14. Same as Figure 12, with $\hbar = 0.02$. Note that the E states were not obtainable due to computational intractability.

Figure 15. Plot of the function $\hbar \ell n\, k$ versus energy for various values of $\hbar$, for the A_1 states. Points are the exact quantum mechanical values (connected with solid lines). The $\hbar = 0$ solid curve is the $\hbar = 0$ limit of the RRKM + tunneling rate, Eq. (2.20b).

Figure 16. Same as Figure 15, for the A_2 states.

Figure 17. Same as Figure 12, for the one-barrier Henon-Heiles potential of Eq. (2.21a), for $\hbar = 0.03$. The solid points denote even transverse states, the circles denote odd transverse states.

Figure 18. The potential energy profile $V(s)$ for the resonance scattering situation of section III.A. s_1, s_2, and s_3 denote the classical motion turning points associated with the analysis leading to the S-matrix.

Figure 19. The first three "amplitude trajectories" which contribute to the overall scattering process. The amplitudes associated with them are given by Eqs. (3.3a), (3.3b), and (3.3c), respectively.

Figure 20. State-specific unimolecular decay rates as a function of energy, as calculated by the branching model, for the one-barrier Henon-Heiles system. Solid points correspond to even states with respect to reflection across the x-axis, circles correspond to odd states. See Figure 17 for a comparison to the "exact" quantum mechanical results.

Figure 21. The potential energy profile V(s) for the scattering situation leading to the determination of double-well potential energy eigenvalues.

Figure 22. Potential energy profile V(s) for the situation giving rise to complex formation in molecular collision processes.

Figure 23. Formaldehyde's out-of-plane bending mode frequency, ω, as a function of displacement along the reaction coordinate, s, as computed via the reaction path Hamiltonian formalism. Solid curve is the scaled SCF result, dashed curve is the polynomial fit used in the complex scaling calculations (see Eq. (4.5b)).

Figure 24. Potential energy profile $V_o(s)$ for formaldehyde decomposition to molecular products, H_2 and CO. Solid curve is a scaled SCF result, dashed curve is a polynomial fit (see Eq. (4.5a)).

Figure 25. Rate constants as a function of total energy for the metastable states associated with the reduced two-dimensional formaldehyde system, Eq. (4.6). Solid points denote even out-of-plane bending states, circles denote odd out-of-plane states.

Figure 26. Rate constants as a function of energy for the three degree of freedom system of Eq. (4.8), holding ω_y constant (i.e., no coupling to y-mode).

Figure 27. Same as Figure 26, but holding ω_x constant (i.e., no coupling to x-mode).

Figure 28. Same as Figure 26, but for the fully coupled system. Note that by superposing the results of Figures 26 and 27, the results shown here are reproduced almost identically.

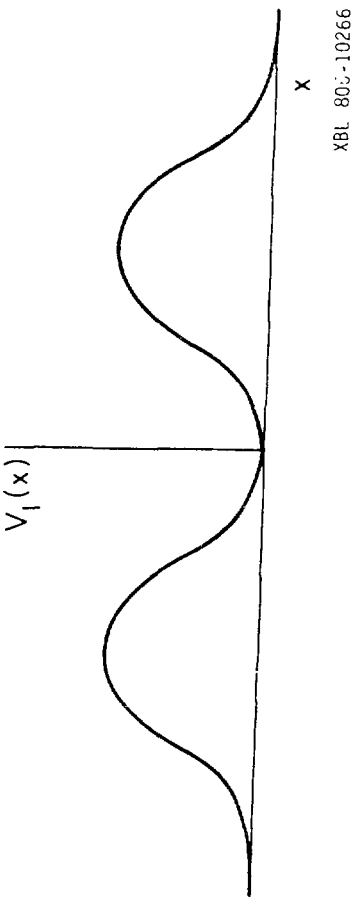

Figure 1

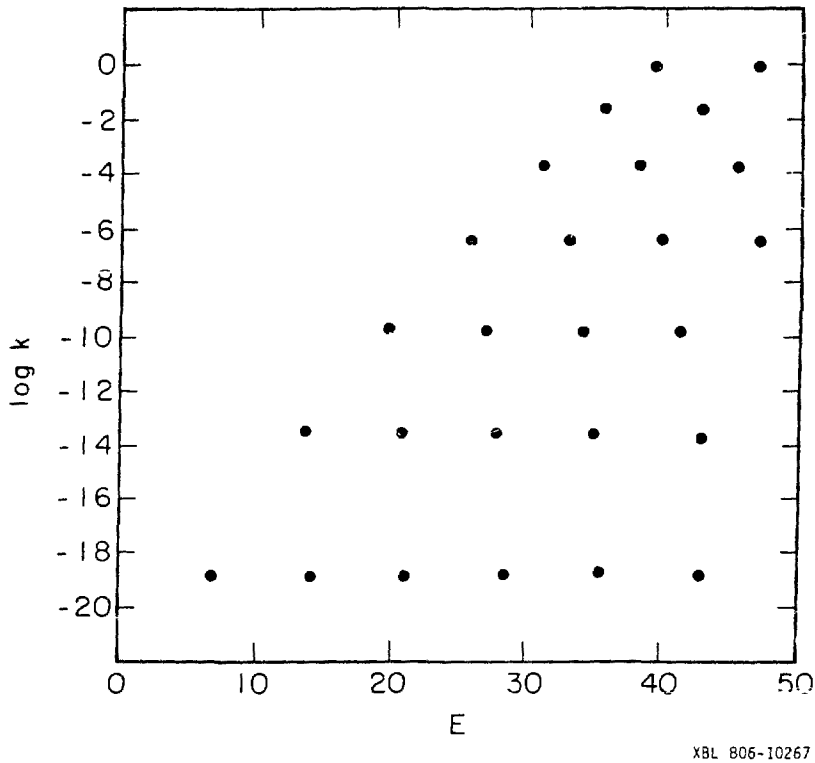

Figure 2

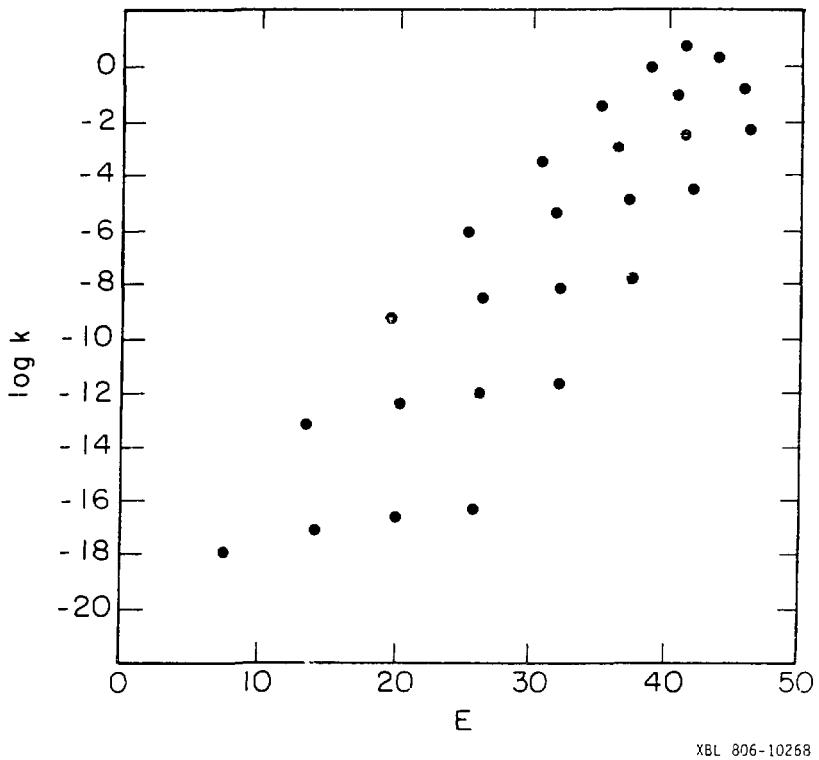

Figure 3

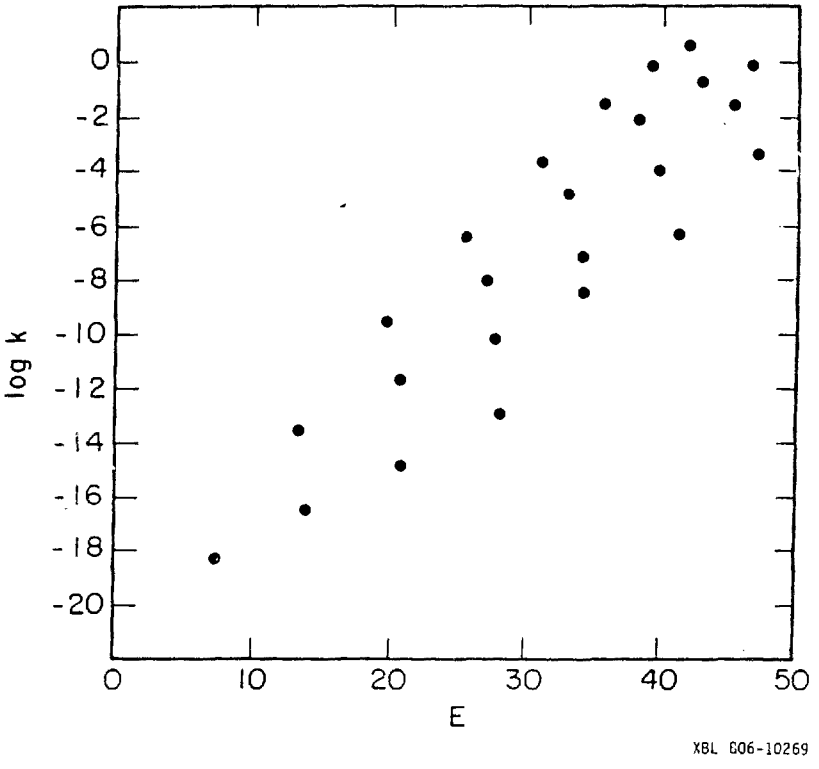

Figure 4

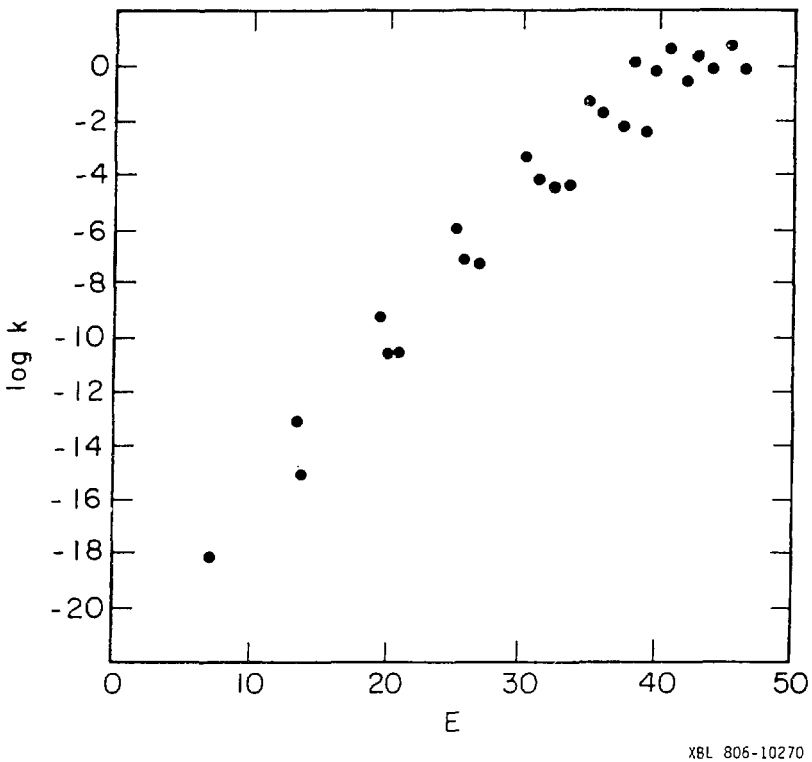

Figure 5

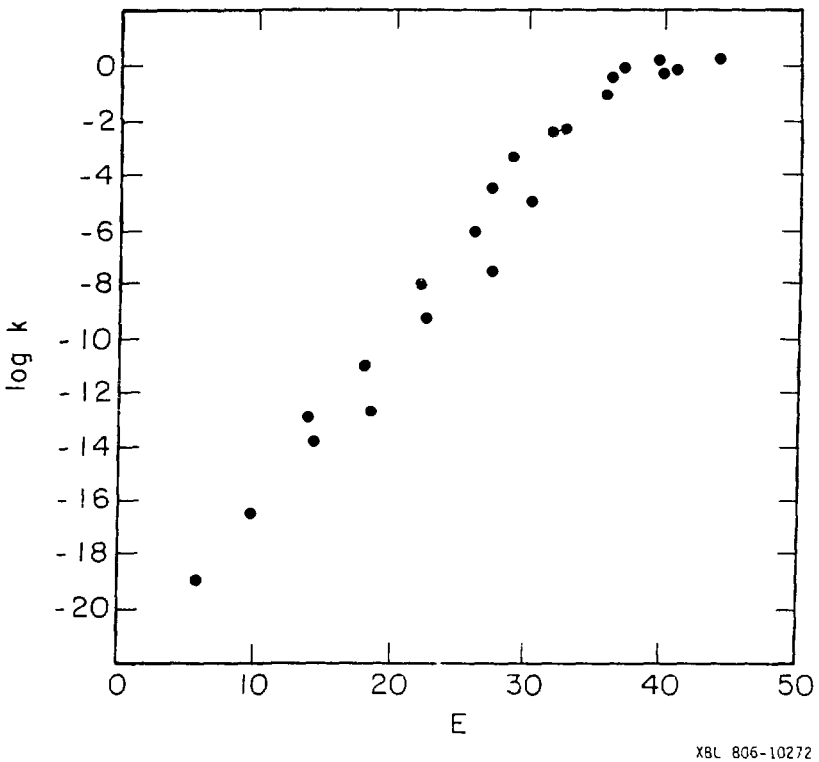

Figure 6

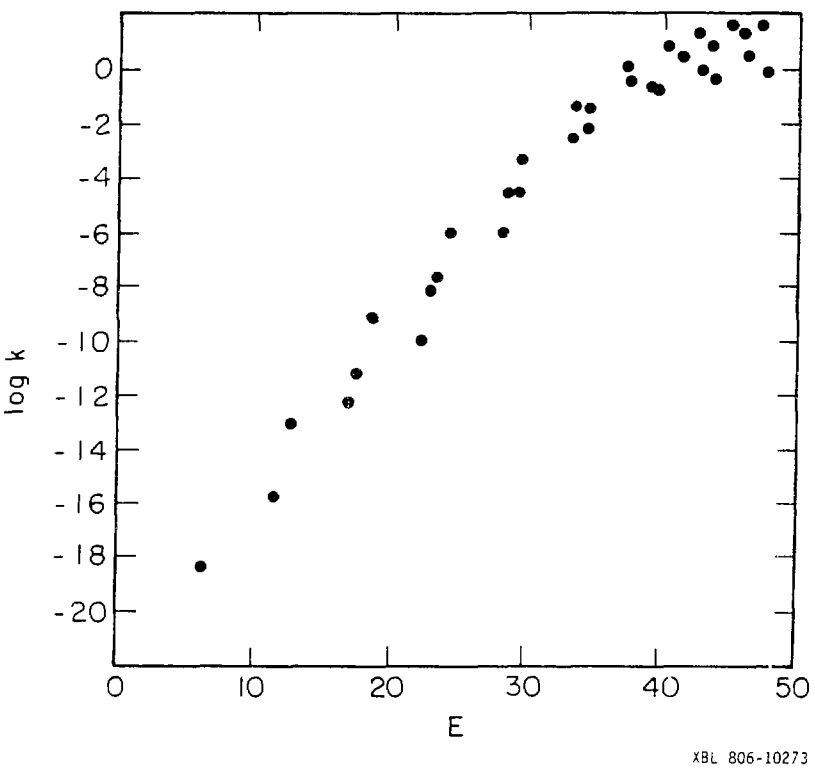

Figure 7

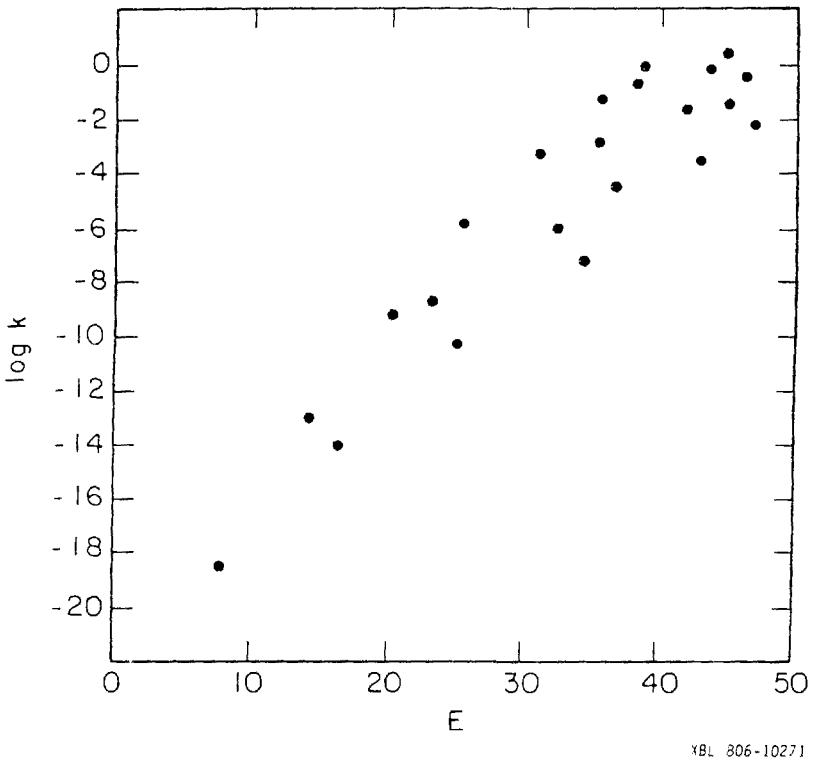

Figure 8

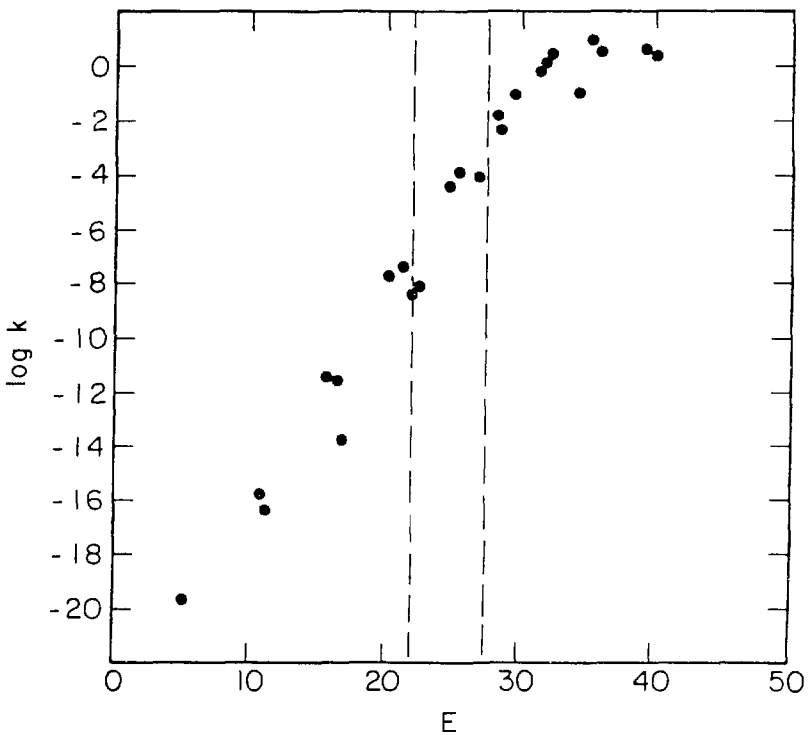

Figure 9

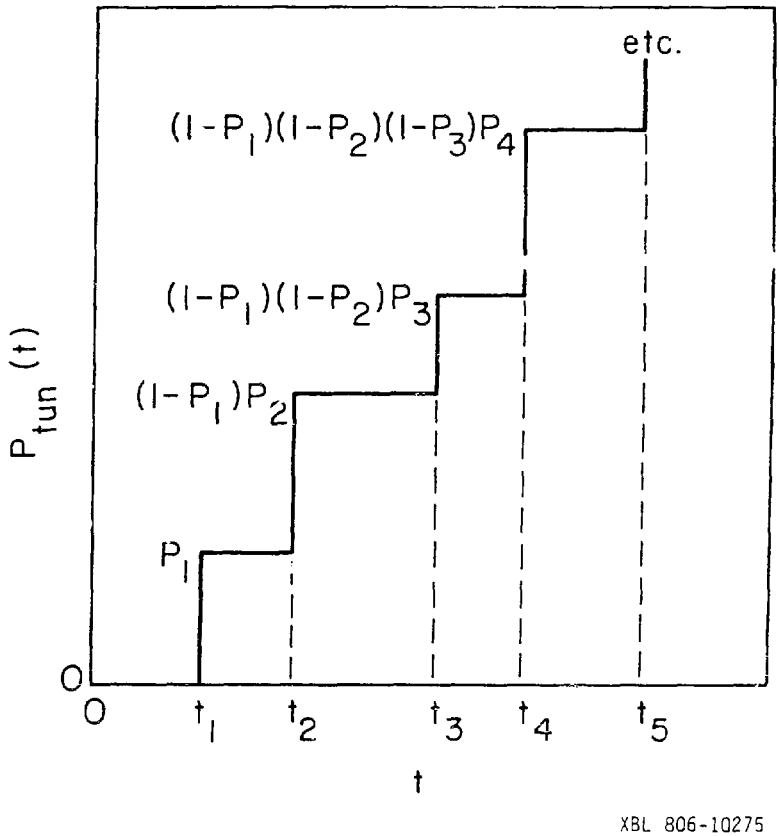
etc.
$(1-P_1)(1-P_2)(1-P_3)P_4$
$(1-P_1)(1-P_2)P_3$
$(1-P_1)P_2$
P_1
$P_{tun}(t)$
0
0
t_1
t_2
t_3
t_4
t_5
t
XBL 806-10275

Figure 10a

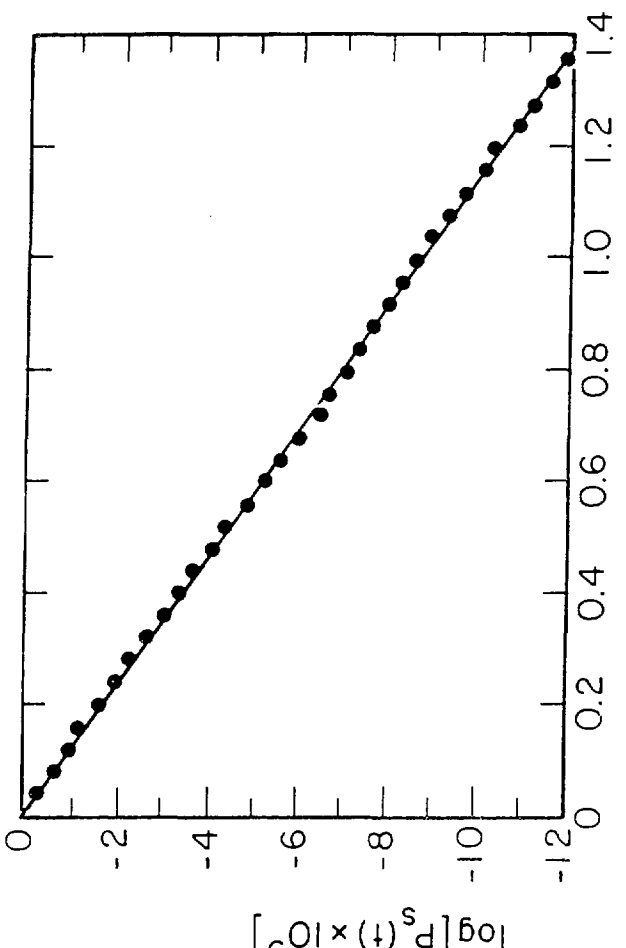

Figure 10b

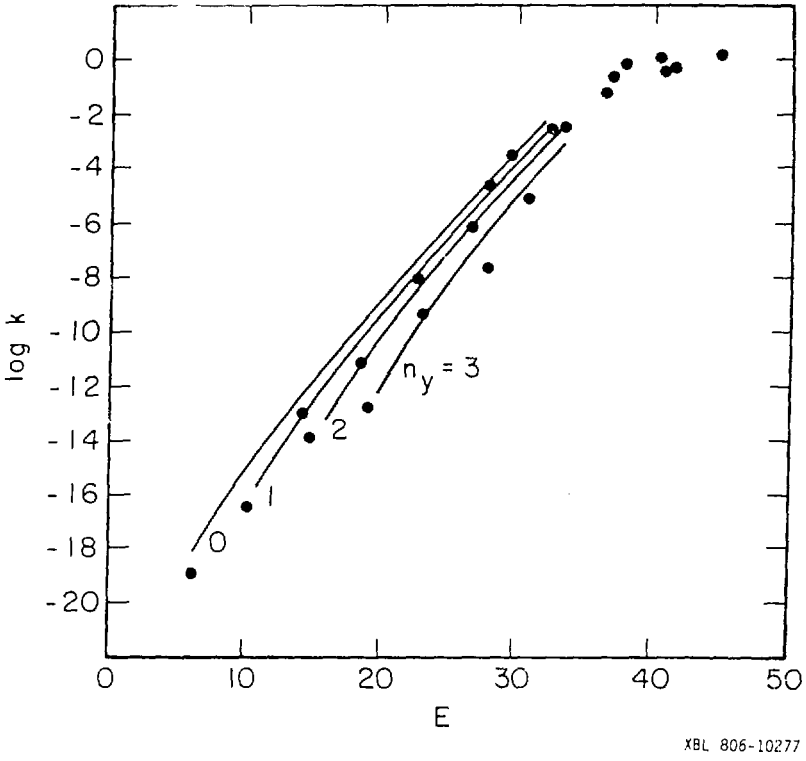
0
-2
-4
-6
-8
-10
-12
-14
-16
-18
-20
log k
0
10
20
30
40
50
E
$n_y = 3$
2
1
0
XBL 806-10277

Figure 11

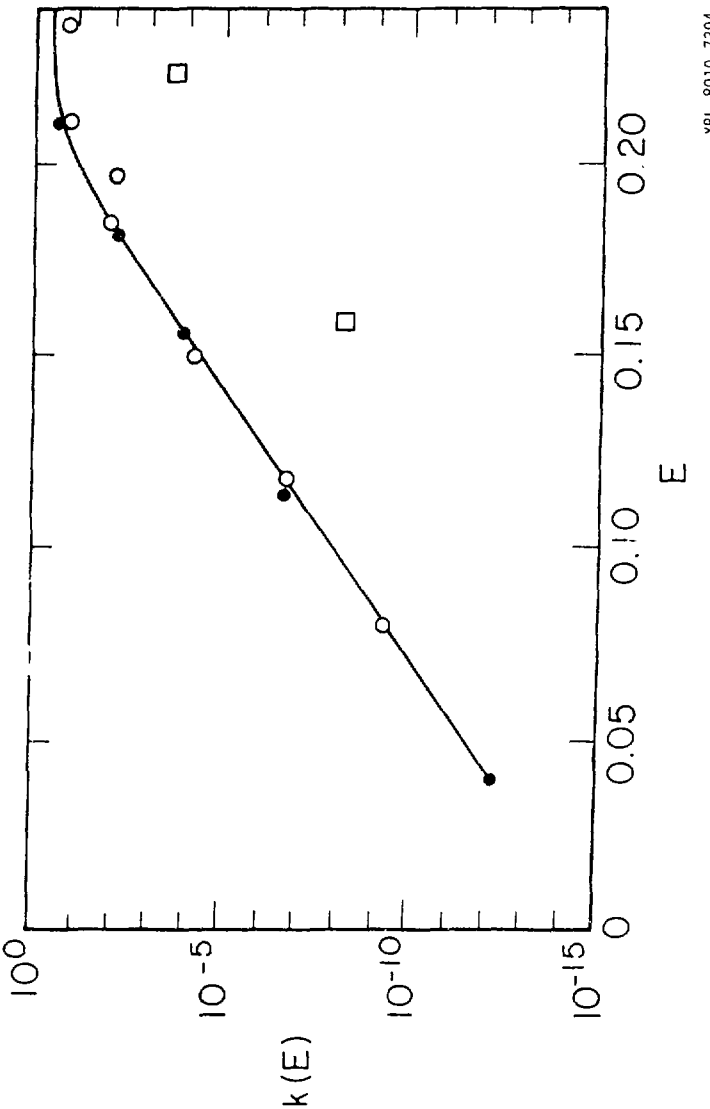

Figure 12

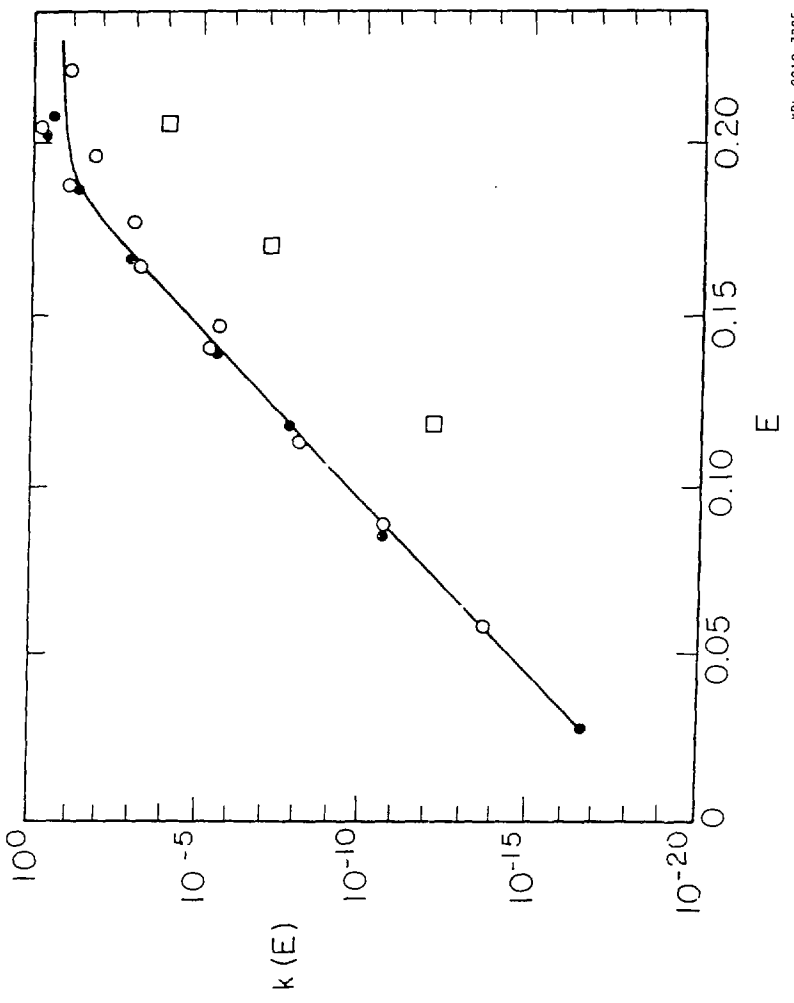

XBL 8010-7395

Figure 13

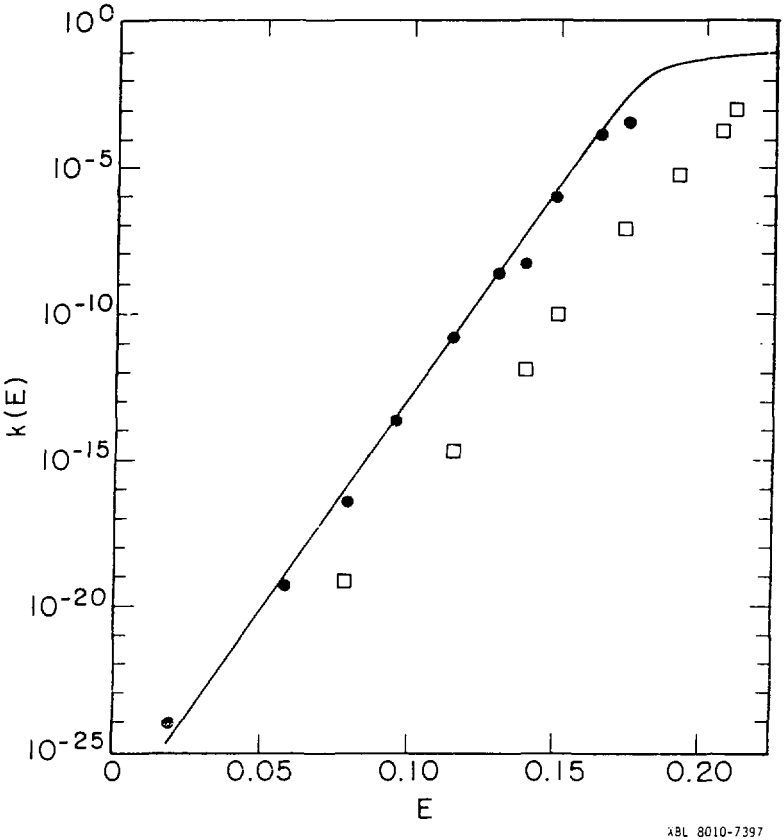

Figure 14

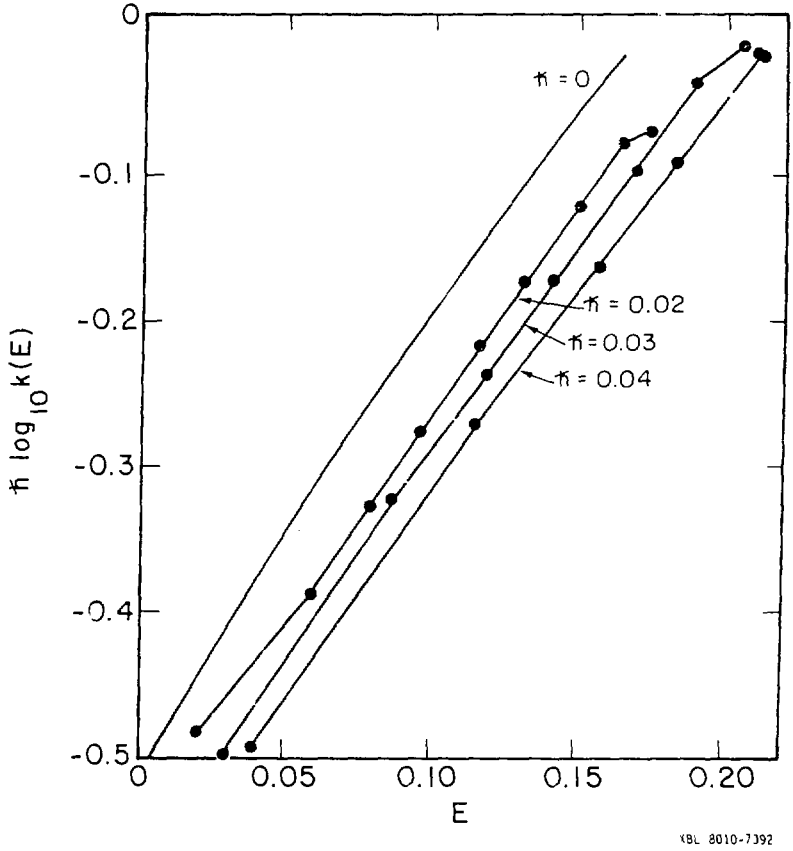
0
-0.1
-0.2
-0.3
-0.4
-0.5
0
0.05
0.10
0.15
0.20
E
ħ log10 k(E)
ħ = 0
ħ = 0.02
ħ = 0.03
ħ = 0.04
XBL 8010-7392

Figure 15

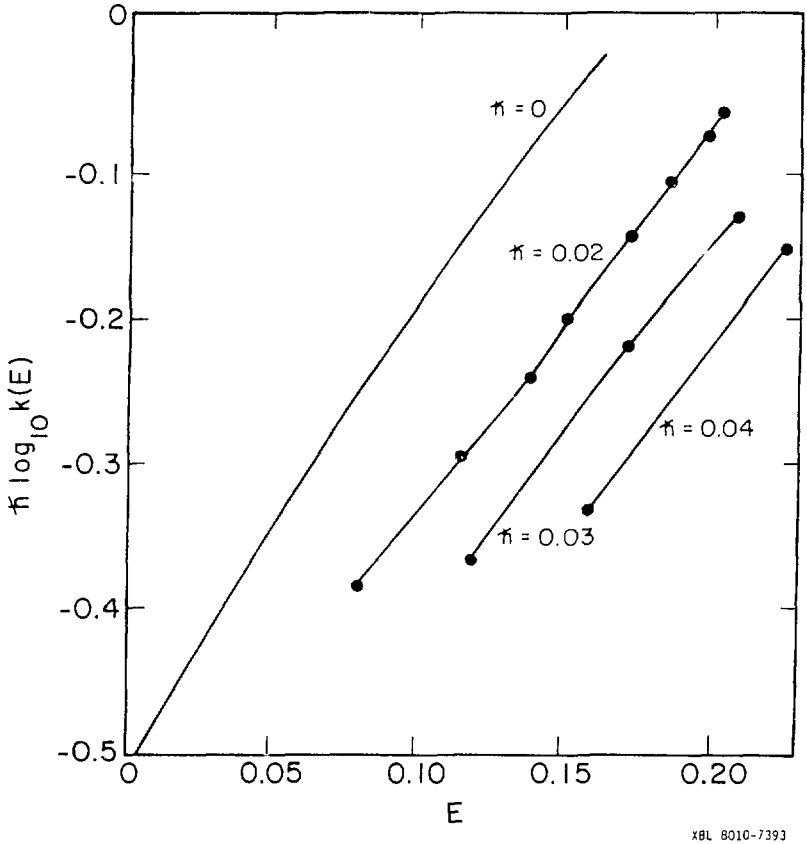
0
-0.1
-0.2
-0.3
-0.4
-0.5
0
0.05
0.10
0.15
0.20
E
ħ log10 k(E)
ħ = 0
ħ = 0.02
ħ = 0.03
ħ = 0.04
XBL 8010-7393

Figure 16

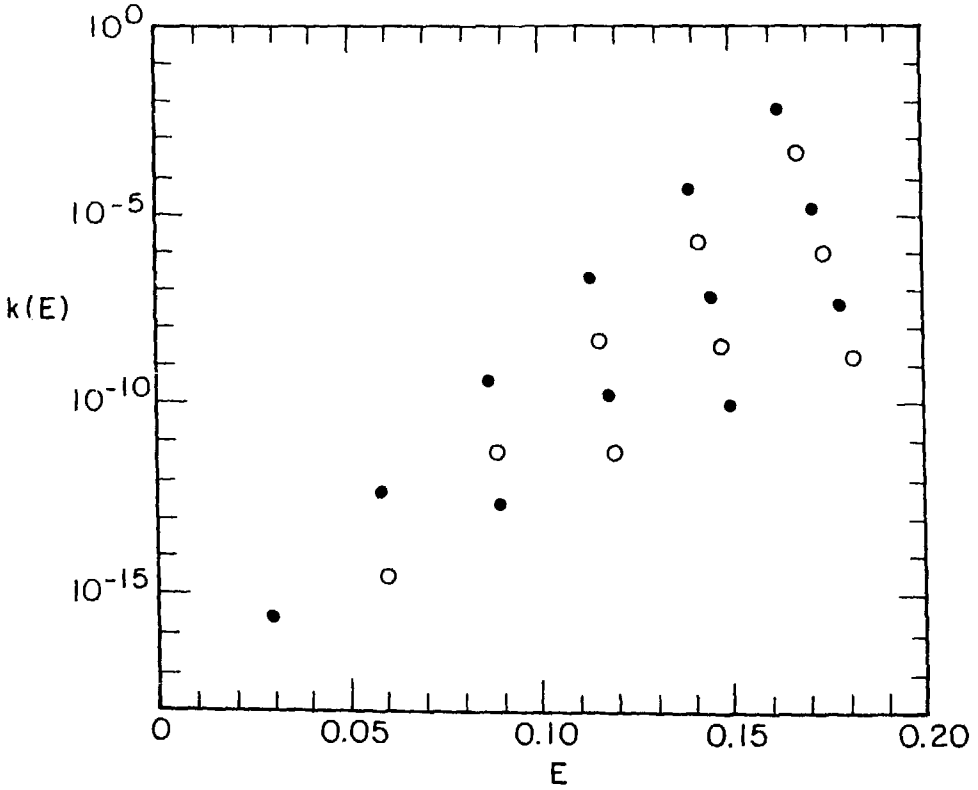

Figure I7

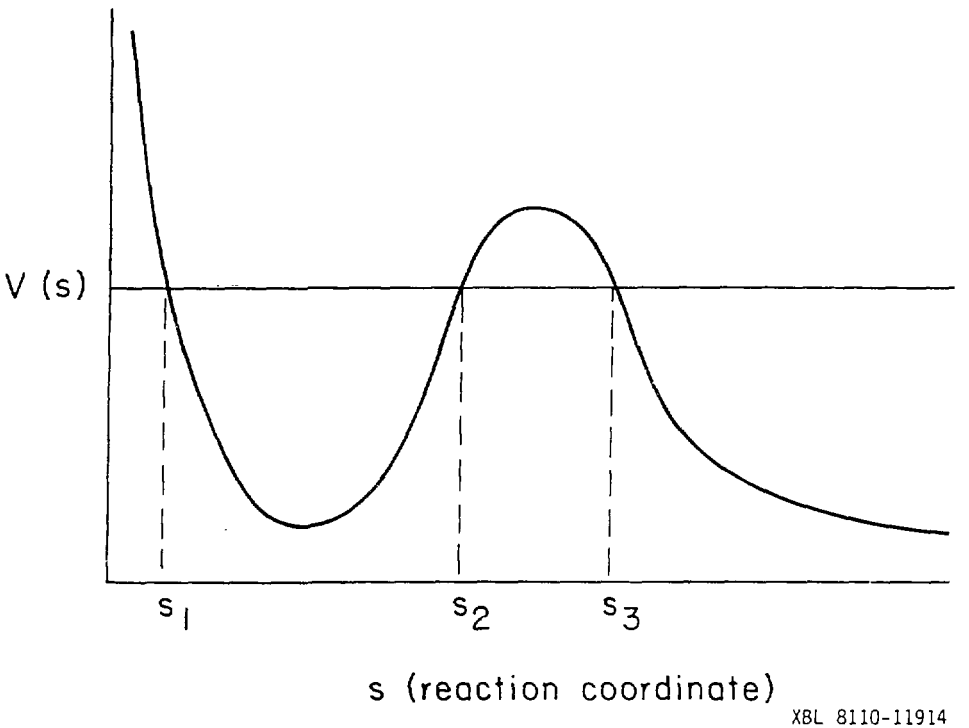

Figure 18

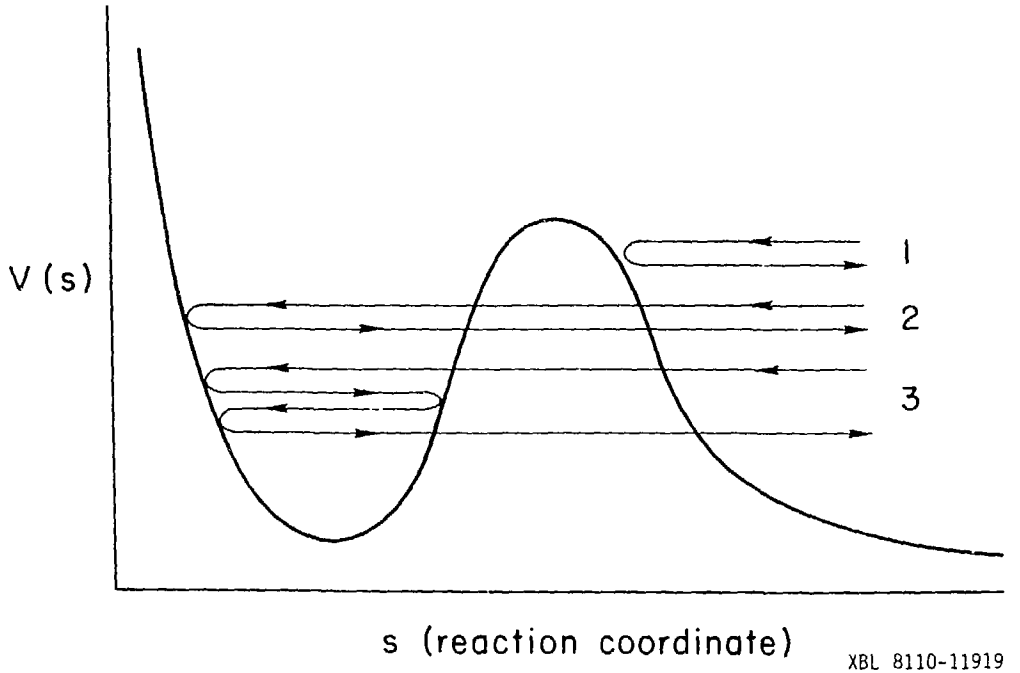

Figure 19

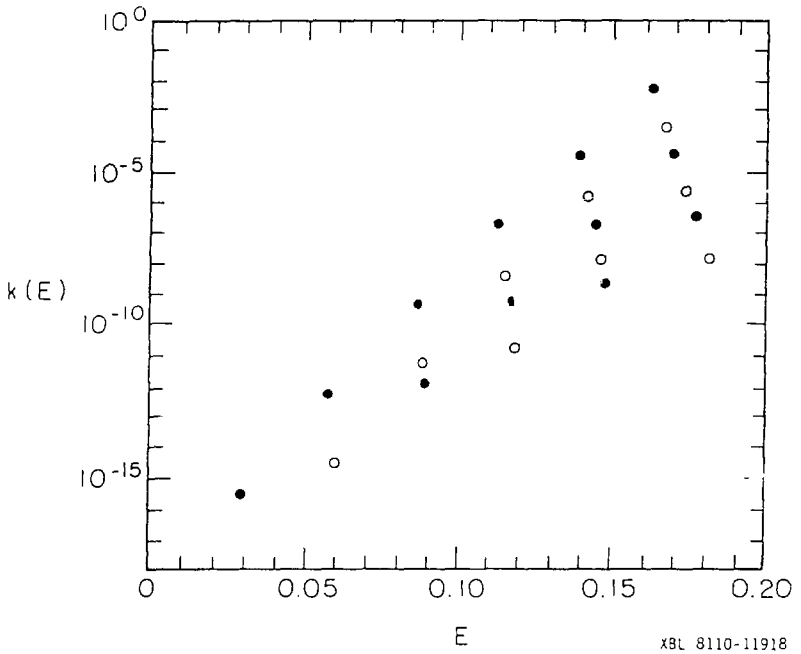

Figure 20

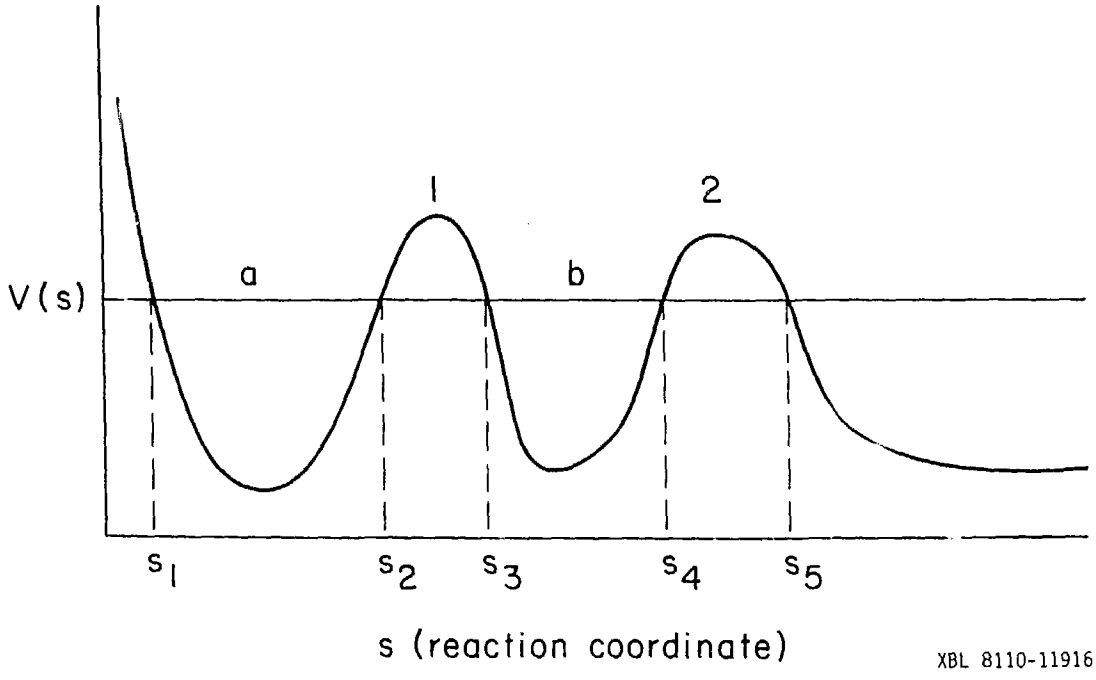

XBL 8110-11916

Figure 21

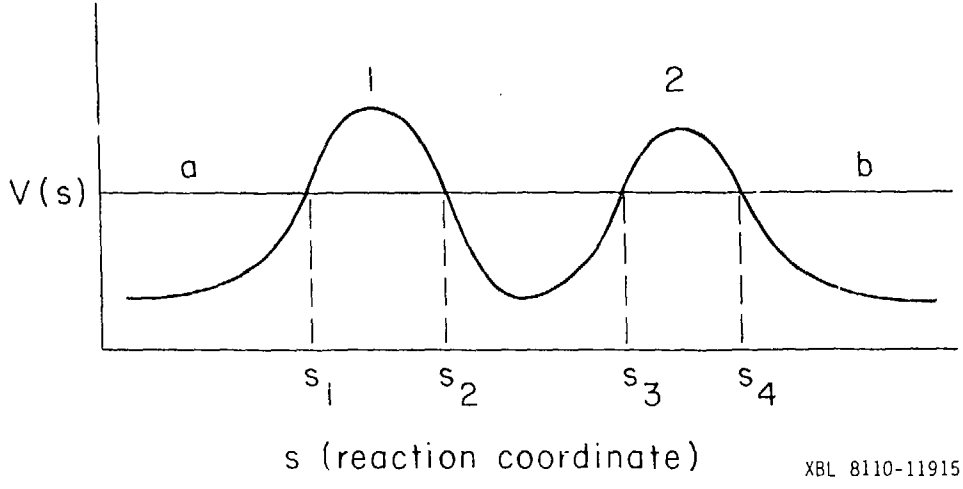

XBL 8110-11915

Figure 22

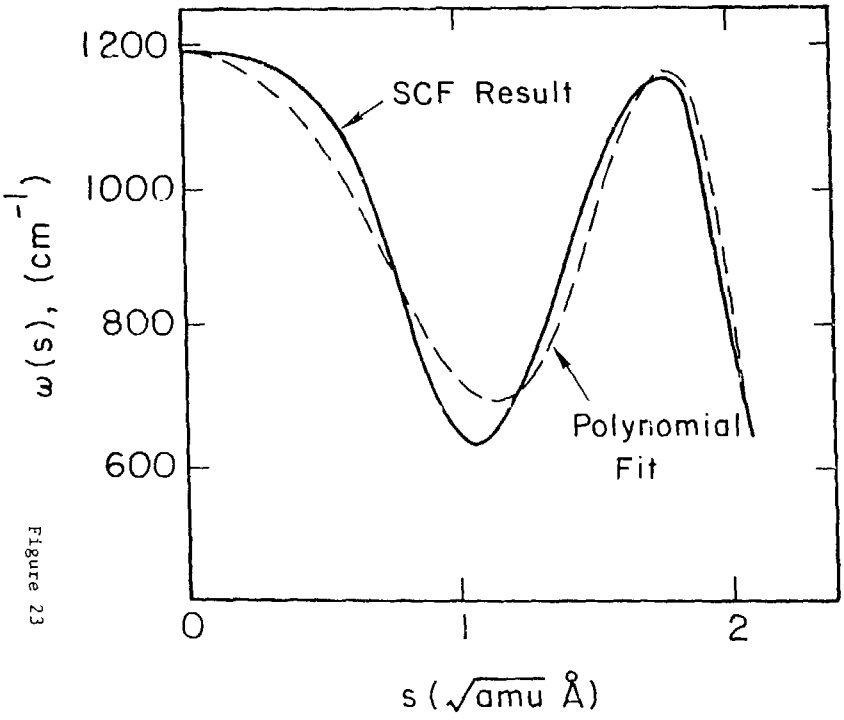

Figure 23

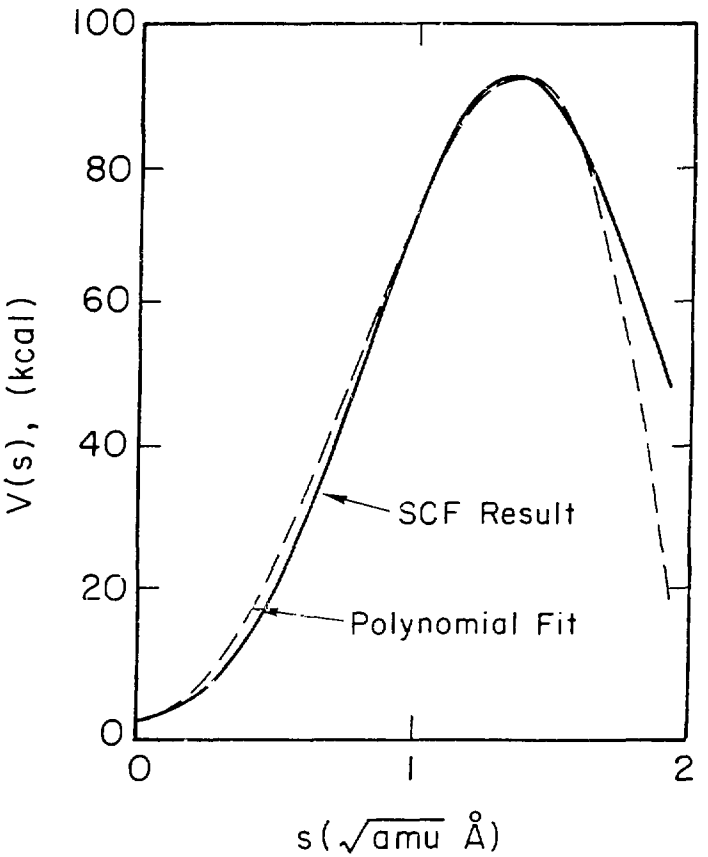

Figure 24

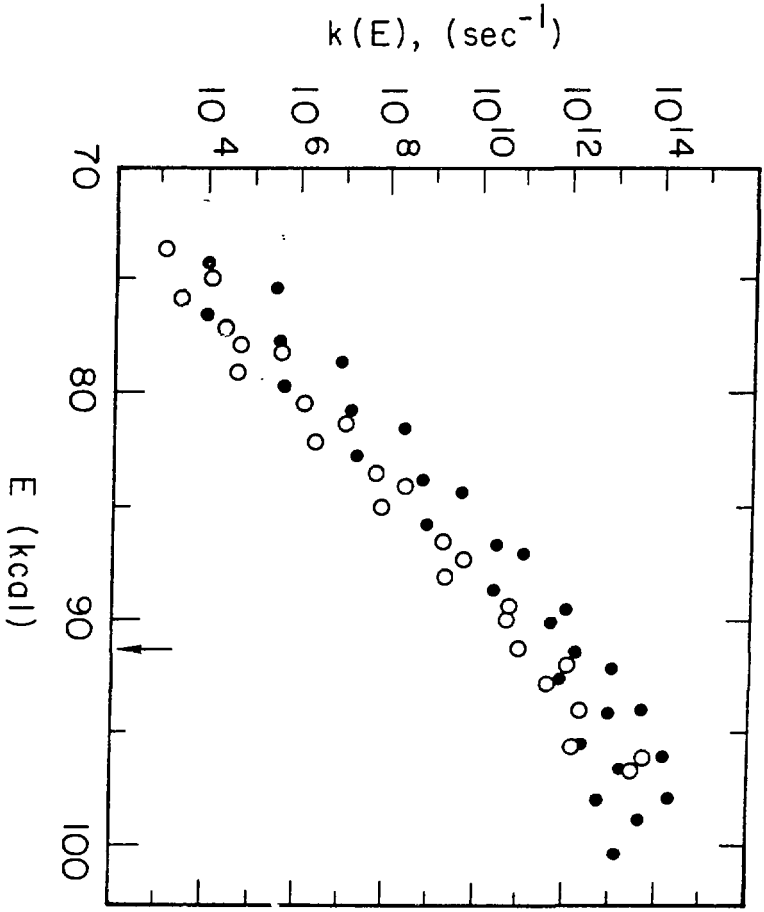

Figure 25

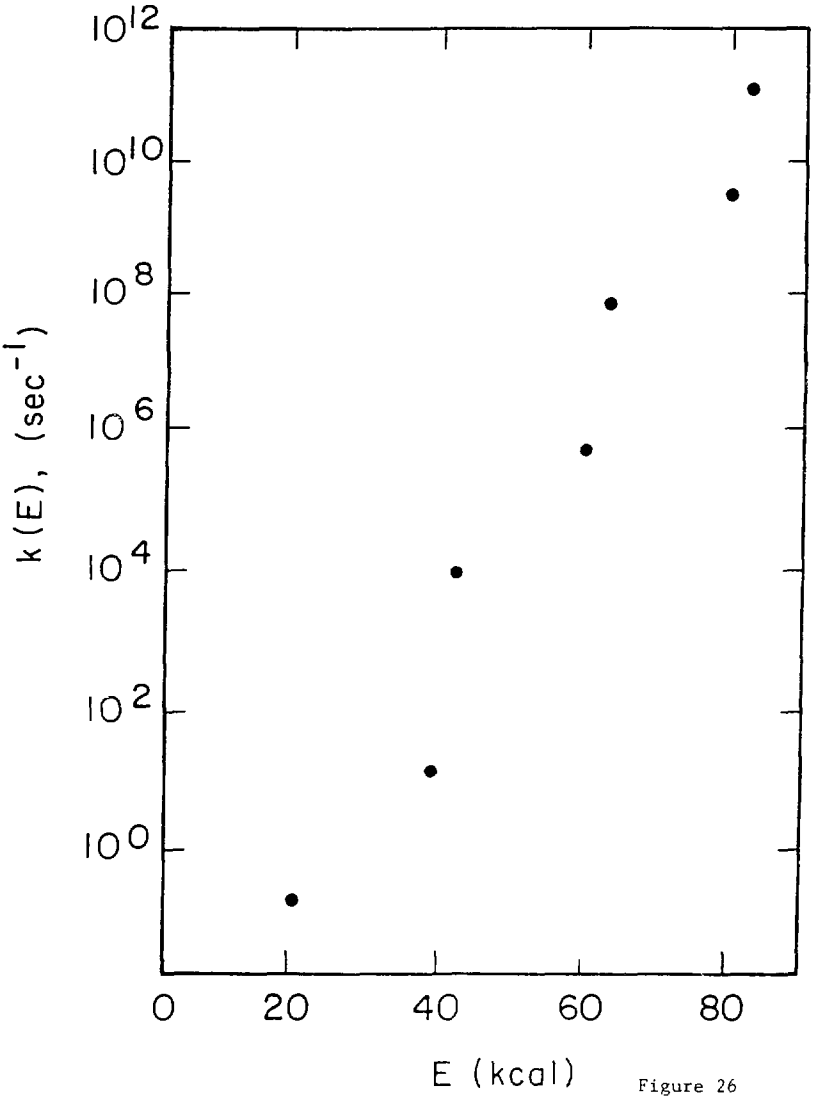

Figure 26

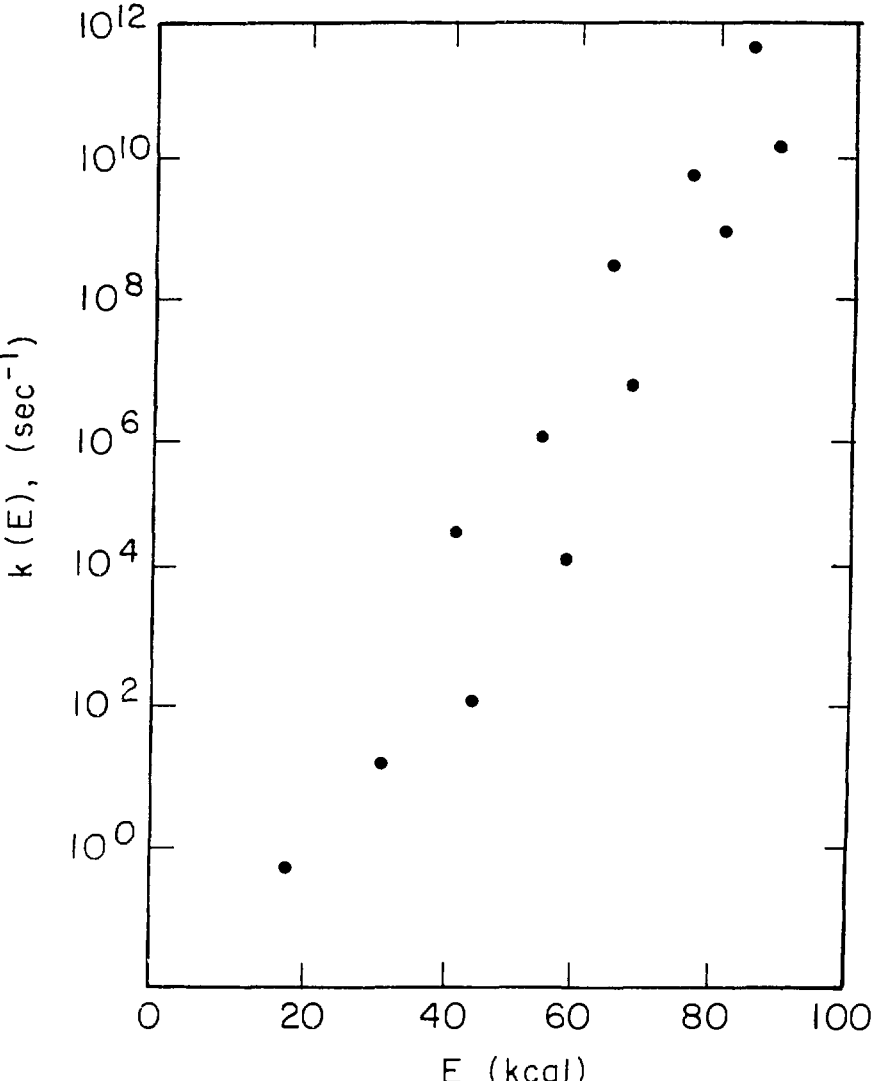

Figure 27

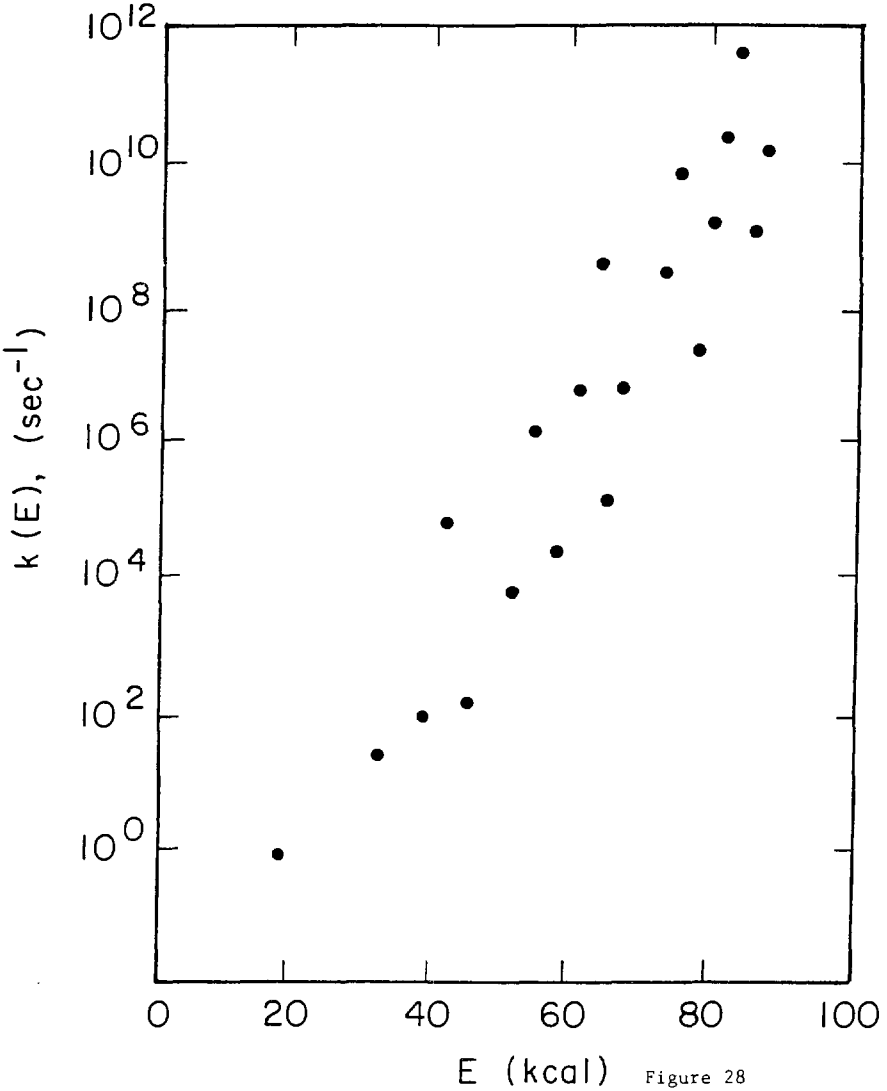

Figure 28